Ayşenur BİÇER

A Master's Thesis

AGU 2023

DEVELOPING HIGH BRIGHTNESS QUANTUM DOT LED DEVICES

A THESIS
SUBMITTED TO THE DEPARTMENT OF ELECTRICAL AND COMPUTER ENGINEERING
AND THE GRADUATE SCHOOL OF ENGINEERING AND SCIENCE
OF ABDULLAH GUL UNIVERSITY
IN PARTIAL FULFILLMENT OF THE REQUIREMENTS
FOR THE DEGREE OF
MASTER OF SCIENCE

By
Ayşenur BİÇER
June 2023

DEVELOPING HIGH BRIGHTNESS QUANTUM DOT LED DEVICES

A THESIS
SUBMITTED TO THE DEPARTMENT OF ELECTRICAL AND COMPUTER ENGINEERING
AND THE GRADUATE SCHOOL OF ENGINEERING AND SCIENCE OF ABDULLAH GUL UNIVERSITY
IN PARTIAL FULFILLMENT OF THE REQUIREMENTS
FOR THE DEGREE OF
MASTER OF SCIENCE

By

Ayşenur BİÇER

June 2023

SCIENTIFIC ETHICS COMPLIANCE

I hereby declare that all information in this document has been obtained in accordance with academic rules and ethical conduct. I also declare that, as required by these rules and conduct, I have fully cited and referenced all materials and results that are not original to this work.

Name-Surname: Ayşenur BİÇER

Signature :

REGULATORY COMPLIANCE

M.Sc. thesis titled Developing High Brightness Quantum Dot LED Devices has been prepared in accordance with the Thesis Writing Guidelines of the Abdullah Gül University, Graduate School of Engineering & Science.

Prepared By	Advisor
Ayşenur BİÇER	Prof.Dr. Evren MUTLUGÜN

Head of the Electrical and Computer Engineering Program

Assoc. Prof. Zafer AYDIN

ACCEPTANCE AND APPROVAL

M.Sc. thesis titled Developing High Brightness Quantum Dot LED Devices and prepared by Ayşenur BİÇER has been accepted by the jury in the Electrical and Computer Engineering Graduate Program at Abdullah Gül University, Graduate School of Engineering & Science.

13 /06/2023

(Thesis Defense Exam Date)

JURY:

Advisor : Prof.Dr. Evren MUTLUGÜN

Member : Asst. Prof. Talha ERDEM

Member : Asst. Prof. Yusuf KELEŞTEMUR

APPROVAL:

The acceptance of this M.Sc. thesis has been approved by the decision of the Abdullah Gül University, Graduate School of Engineering & Science, Executive Board dated ….. /….. / …….. and numbered ……..……. .

…….. /…….. / ……..

(Date)

Graduate School Dean

Prof. Dr. İrfan ALAN

ABSTRACT

DEVELOPING HIGH BRIGHTNESS QUANTUM DOT LED DEVICES

Ayşenur BİÇER

MSc. in Electrical and Computer Engineering

Advisor: Prof.Dr. Evren MUTLUGÜN

June 2023

Optoelectronic devices are essential components of optical communication systems, internet and displays. Among these devices, in the category of light emitting diodes (LED), there are quantum dot LEDs (QLED) that emit light by employing quantum dots (QDs) and have rich optoelectronic properties such as varying emission wavelength associated with the its size and excellent brightness [1], [2]. In this thesis, we worked on transparent and solution processible QLEDs in three groups: Indium Phosphide (InP) QLEDs, Carbon Quantum Dot (CQD) LEDs and Cadmium Selenide (CdSe) QLEDs. In the InP study, a QLED was fabricated using InP-based QDs as the emitting layer to demonstrate the feasibility of these QDs. Results found a maximum external quantum efficiency (EQE) of 1.16% and brightness of 1039 cd/m^2. For the CQD LEDs, yellow emissive QDs were mixed systematically in Poly(9-vinylcarbazole) (PVK) as the host. A blue-to-white shift was observed in the CIE coordinate with varying ratios. From these, white luminescent devices were obtained with a maximum brightness of 774.3 cd/m^2 and an EQE of 0.76%. High-brightness irradiation was obtained compared to other white-luminescent studies in the literature. In CdSe QLEDs, as a proof of concept, devices with a maximum brightness of 111,450 cd/m^2 and an EQE of 15.08% were obtained. In these three works, devices with high brightness in their own categories were produced using both heavy metal and non-heavy metal QDs.

Keywords: Optoelectronics, LED, QD, CQD LED, InP QLED, CdSe QLED

ÖZET

YÜKSEK PARLAKLIK KUANTUM NOKTA LED AYGITLARIN GELİŞTİRİLMESİ

Ayşenur BİÇER

Elektrik ve Bilgisayar Mühendisliği Anabilim Dalı Yüksek Lisans

Tez Yöneticisi: Prof.Dr. Evren MUTLUGÜN

Haziran 2023

Optoelektronik cihazlar, optik iletişim sistemlerinin, internetin ve ekranların temel bileşenleridir. Bu cihazlar arasında, ışık yayan diyotlar (LED) kategorisinde, kuantum noktalar (KN'lar) kullanarak ışık yayan ve boyutuna bağlı emisyon dalga boyu değişen, zengin optoelektronik özelliklere sahip olan kuantum nokta LED'ler (KN LED) bulunmaktadır. parlaklık [1], [2]. Bu tezde şeffaf ve solüsyon formunda işlenebilir KN LED'ler üzerinde üç grupta çalıştık: İndiyum Fosfit (InP) QLED'ler, Karbon Kuantum Nokta (CQD) LED'ler ve Kadmiyum Selenid (CdSe) KN LED'ler. InP çalışmasında, bu QD'lerin fizibilitesini göstermek için ışıyıcı katman olarak InP tabanlı QD'ler kullanılarak bir KN LED üretildi. Sonuçlar, %1,16'lık bir tepe dış kuantum verimliliği (EQE) ve 1039 cd/m^2 parlaklık gösterdi. CQD LED'leri için sarı ışıyan KN'lar sistematik olarak Poli(9-vinilkarbazol) (PVK) içinde karıştırıldı. CIE renk koordinatında değişen karışım oranlarıyla birlikte maviden beyaza kayma gözlendi. Bunlardan maksimum 774,3 cd/m^2 parlaklığa ve %0,76 EQE'ye sahip beyaz ışıyan cihazlar elde edildi. Literatürdeki diğer beyaz-ışıldayan çalışmalara kıyasla yüksek parlaklıkta ışıma elde edilmiştir. CdSe QLED'lerde konsept gösterimi olarak maksimum 111.450 cd/m^2 parlaklığa ve %15,08 EQE'ye sahip cihazlar elde edildi. Bu üç çalışmada ağır metal hem içeren hem de içermeyen KN'lar kullanılarak kendi kategorilerinde yüksek parlaklığa sahip cihazlar üretildi.

Anahtar Kelimeler: Optoelektronik, LED, Kuantum Nokta, Karbon KN LED, InP KN LED, CdSe KN LED

Acknowledgements

First, I would like to express my sincere thanks to my advisor, Professor Doctor Evren MUTLUGÜN, who always guided me and provided financial and emotional support throughout my graduate studies. I owe thanks to Asst. Prof. Talha ERDEM, who always helped me with patience, and a smiling face, like a second advisor during this time.

I would also like to thank Prof. Dr. Mustafa Serdar ÖNSES, who provided financial support through the TÜBİTAK project, and to Prof. Dr. Hakan USTA, who always supported us and tried to teach what he knew in the best possible way.

I feel lucky to have the opportunity to work with knowledgeable and experienced scientists like you. There have been many teachings that I have learned from you since my undergraduate education, both academically and personally. I hope to be an instructor like you.

Thanks to my colleague Ahmet Faruk YAZICI for his valuable feedback, material support and answers to my questions throughout my studies. I would like to give an emotional thank you to Asst. Prof. Kevser ŞAHİN TIRAŞ, who conveyed her valuable experiences to me under all circumstances throughout our joint work. Thanks, Müzeyyen SAVAŞ, with whom we walked along my master's path, and my colleagues Dr. Ehsan SOHEYLİ, Dr. Sema KARABEL ÖCAL, Zeynep ŞENEL, İbrahim Furkan TEZCAN and Muhammad Fuad FAROOQİ, who provided support when I needed it.

I would also like to thank TÜBİTAK for financial support with projects numbered 119F384 and 20AG026 throughout my studies.

Finally, the most precious ones are my altruist parents İbrahim ARSLAN and Fatma ARSLAN, my dear husband Mürşit Alperen BİÇER, my sweetheart siblings Batuhan ARSLAN and Aylin ARSLAN. Thank you so much for always being there for me, believing in me, and providing the peaceful environment I need.

TABLE OF CONTENTS

TABLE OF FIGURES

LIST OF TABLES

LIST OF ABBREVIATIONS

QD	Quantum Dot
QLED	Quantum Dot Light Emitting Diode
CTL	Charge Transport Layer
HIL	Hole Injection Layer
HTL	Hole Transport Layer
ETL	Electron Transport Layer
ZnO	Zinc Oxide
NP	Nanoparticle
InP	Indium Phosphide
CQD	Carbon Quantum Dot
CdSe/ZnS	Cadmium Selenide/Zinc Sulfide

To ARSLAN and BİÇER families

Chapter 1

Introduction

Light is an electromagnetic wave. There are different types in the point electromagnetic spectrum depending on the wavelength of the wave. Among these species, the 380–750 nm (Figure 1.1) range is the visible light region, and the human eye can detect this light. There is a scale ranging from blue to red in the visible light region. The QLED devices mentioned in this thesis are devices that radiate in the visible light region.

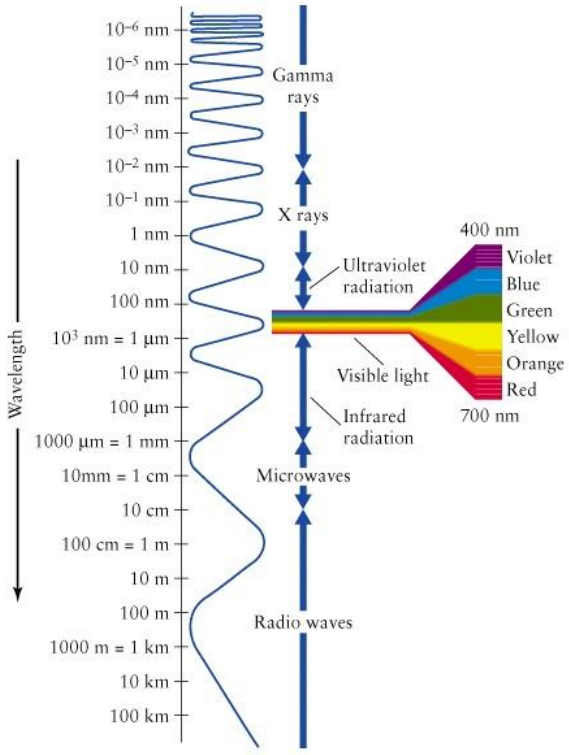

Figure 1.1 Electromagnetic spectrum [3]

Optoelectronic devices that can convert electrical and optical signals to each other are used in almost every field of work, especially displays commonly used in daily life. Examples of optoelectronic devices are photodetectors, laser diodes, and light emitting diodes (LEDs) [4], [5]. These devices convert electrical/optical signals into each other. Among them, LEDs, which convert electrical input to optical output (light), are quite common in daily life with many versions. In particular, devices with high brightness and wide color gamut have been produced with LEDs using quantum dot (QD) nanoparticles as an emissive layers [6], [7]. It has a wide usage potential, especially in display technologies commercialised as QLED TVs, which are demanded in technology markets, to military applications. High brightness, color diversity and high efficiency are among the basic qualities demanded by the industry in this field .

In addition to these, another important issue is whether QDs contains toxic materials. In this context, Carbon Quantum Dots stand out with their non-toxicity, nature-friendly, low cost and optoelectronic properties [8]. Another type of quantum dot that is non-toxic, efficient than carbon dots are indium phosphide quantum dots [9]. However, highly luminescent CdSe QDs, although toxic, have been extensively studied in the literature. extensively studied in the literature [9].

CdSe QDs in terms of containing toxic semiconductor material, InP QDs in terms of containing non-toxic semiconductor material and CQDs in terms of non-toxic and non-semiconductor based QDs have been studied in the QLED device structure. We carried out studies in the laboratory of Abdullah Gül University to develop and diversify quantum dot LEDs with these important features.

Chapter 2

Quantum Dots

2.1 Semiconductor Nanoparticles

With the bulk materials that came to the fore in the historical development process and subsequent molecular studies, nanoparticles in the medium-sized form of these two and with their extraordinary properties are one of the most popular topics of recent times. The general definition of nanostructures is that they are in the range of 1-100 nm in at least one of the 3 dimensions. In this context, all 3 dimensions larger than 100 nm are grouped as 3d and are called bulk materials. Those that are greater than 100 nm in 2 dimensions and are in this range in only 1 dimension are in the 2d group, those that are larger in 1 dimension and in this range in 2 dimensions are in the 1d group and those in this range are in the 3 dimensions. dimensions are in group 0d. Examples of 2-dimensional nanoparticles are nanoplates, thin films, quantum wells, 1-dimensional nanofibers, and 0-dimensional quantum dots (QD) (Figure 2.1C).

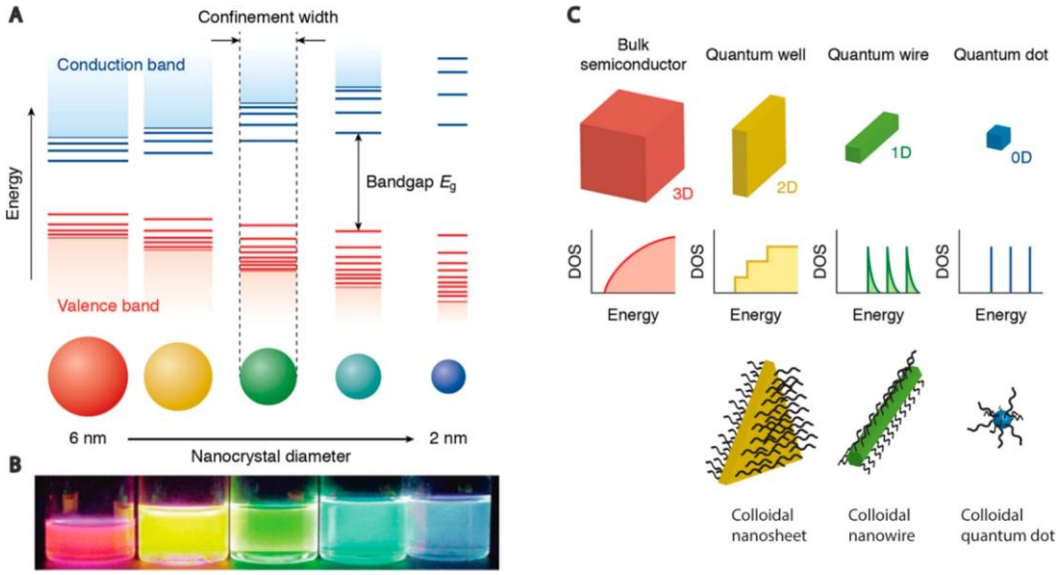

Figure 2.1 A) The consequences of quantum confinement. B) UV-illuminated colloidal mixes of NCs in a range of dimensions. C) The energy level structures for bulk semiconductor, 2D, 1D, and 0D NCs, along with examples of each.[10]

Semiconductor nanostructures have potential applications in many fields thanks to their unique optical, electrical, and mechanical properties, which are given by the size limitations. Colloidal semiconductor nanocrystals (NCs), which are tunable nanomaterials, vary in size, shape, composition, and compositional profile (Figure 2.1A and Figure 2.1B), which influences their optoelectronic properties. The cause of the size and shape dependence of their features is the structural confining of charge carriers and excitons in the material itself, which results in quantum confinement effects [10].

On the outside of the nanocrystals are ligand molecules. These molecules are effective in gaining some characteristic features such as size and shape of nanocrystals. Thus, materials with different identities can be obtained together with the tunable feature that can provide variability [10]. Although this potential weakens in toxic material-based structures, it has been possible to produce non-toxic nanoparticle alternatives such as InP, InSb, $CuInS_2$ [10].

2.2 Quantum Dots

Quantum Dots are nanoparticles in the 0D group of semiconductors and are confined in 3 dimensions. It can change color according to size properties and has a narrow full-width half maximum (FWHM). When these QDs are used as a emitter in the device structure, they affect the quality of the device, so that the desired color can be adjusted, and it emits pure colors. They are small structures made up of a certain number of atoms with discreate energy levels compared to bulk structures.

The motion of electrons and holes is physically restricted to the dimensions of the QD when the semiconductor nanocrystal's radius has a value equal to or smaller than the exciton Bohr radius [1]. Furthermore, the mobility of charges in the crystal is constrained when the energy gap between two QD levels approaches the value k_BT where k_B and T are the Boltzmann constant and temperature in Kelvins, respectively [11]. The NCs' free energy increases, making them more reactive and dynamic than their bulk counterparts when their surface to volume ratio increased. As a result, it changes the material's basic properties, including its ability to dissolve, reactive properties, evaporation and melting temperature, flexibility, etc.[11].

Utilizing the structural variations of quantum dots is one way to categorize them. Three types of quantum dots may be distinguished: alloy structure, core-shell, and core.

2.2.1 Core Type

A single sort of chemical molecule, such as selenide, sulfide, or telluride, of metals like cadmium, indium, lead, and zinc makes up this kind of quantum dot [12]. These materials with exceptional fluorescence characteristics are commonly employed in fluorescence imaging and biosensing applications [13].

2.2.2 Core-Shell Type

The addition of a shell surrounding the core can improve confinement to the carriers and passivate the surface dangling bonds, enhancing the PL efficiency compared to the

bare QDs, depending on the relative band alignment of the core and shell compositions. The luminous property of quantum dots occurs with the radiative recombination of the electron-hole pair. However, if the energy of the electron-hole pair is transferred by non-radiative recombination (by mechanisms other than radiative coupling), the fluorescence quantum efficiency drops significantly [14]. One of the ways to prevent this loss mechanism and increase the luminous efficiency and brightness is to grow materials with higher energy band gap that will form the shell structure around semiconductor nanoparticles. These enlarged structures passivate the regions on the nanocrystals that will cause non-radiative coupling, increasing the quantum efficiency and making the quantum dots more stable [15], [16]. The core and the shell can have different energy band levels. According to these levels, the quantum dots in the core-shell structure are divided into different categories Figure 2.2.

The shell energy band gap is greater than the core structure in type I structures. Charge carriers are constrained inside the core as a result of the energy barrier around its valence and conduction bands. The photo-excited charge carriers are partially or entirely confined in the shell structure of the reverse-Type I structure. The thickness of the shell may be changed to alter the emission wavelength. In order to increase photostability and fluorescence quantum yield, Type I core/shell quantum dots were investigated [15], [16]. The CdSe/ZnS core/shell configuration is the most often mentioned Type I II-VI semiconductor in the literature [17].

In type II structures, the band gap in the core structure and the conduction or valence band in the shell structure are congruent. The core/shell structure has an isolated area where photo-excited excitons are generated. In circumstances when the conduction band difference is very minimal, unlike the Type I quasi-Type I (quasi) structure that is described in the literature, the wave function of the electrons covers the whole structure while the wave function of the holes is constrained to the core [18].

2.2.3 Alloy Type

The development of semiconductor quantum dots has been greatly aided by alloy architectures, which allow for the modification of optical and electrical characteristics

without affecting the size of the particle. In contrast to other QD types, the material composition of alloy structures progressively shifts as a radial gradient from the center to the surface. On the other hand, since radial variation of the material composition diminishes the lattice mismatch, high efficiency quantum dots may be produced [19].

The core/shell quantum structure is quite common in the literature. The 4 structures shown in Figure 2.2 are different core/shell structures. Type I, type II, quasi type II, and reverse type I are the names of these structures [20]. The gray part on the edges of these tips represents the energy diagram of the shells, and the light blue part represents the energy diagram of the cores. The blue part of the double-sided graph under the structure types is the wave function graph of electrons, and the red graph drawn on the opposite side is those of the holes. Core/Shell QDs may be distinguished based on the difference between the band gap energies (E_g) of the core and the shell.

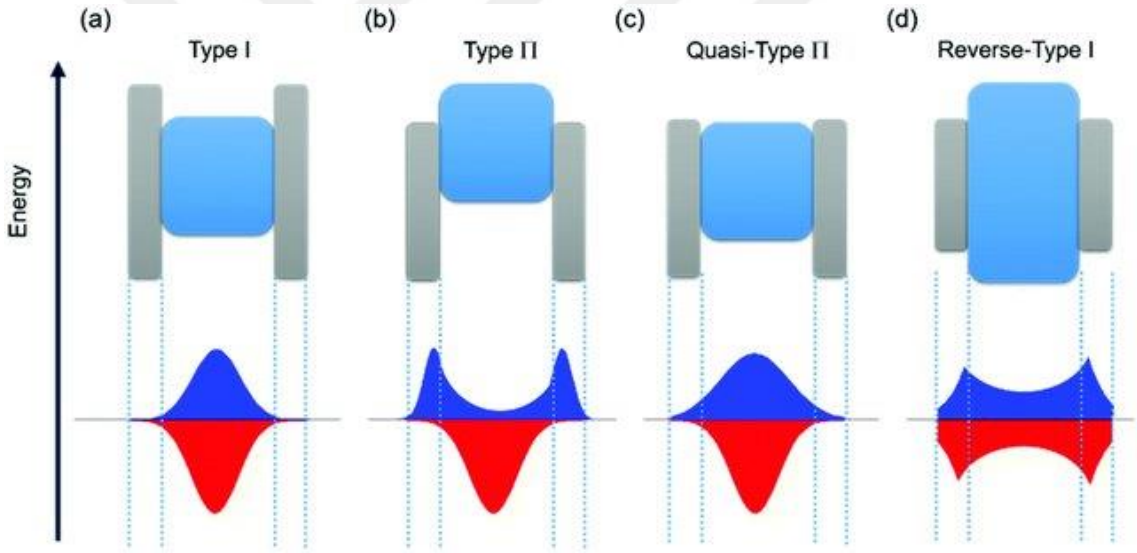

Figure 2.2 Diagrammatic representation of band alignment for several core/shell structures: type I, type II, quasi type II, and reverse type I. Blue symbolizes the wave function that represents electrons, whereas red stands for the wave function that represents electrons, whereas red stands for the wave function that represents holes. [20]

Inorganic semiconductor materials make up the majority of QDs, which are typically made with elements from groups 12–16 of the periodic table (binary II–VI type QDs) and 14–16 (binary IV–VI type QDs). Unary IV type QDs, metal-free elemental QDs, ternary I-III-VI type QDs, and quaternary I-II-IV-VI type QDs are only a few of the

many additional, less well-studied types of quantum dots. Table 2.1 shows sample materials for some of these types of QDs [17].

Table 2.1 QD types and their examples [17]

QD Type	**IV–VI QDs**	**II–VI QDs**	**III–V QDs**	**IV QDs**	**II–V QDs**	**I–VI QDs**	**I–III–VI QDs**	**II–II–VI QDs**
Examples	PbS, PbSe and PbTe	ZnS, ZnSe, ZnTe, CdS, CdSe, CdTe and HgTe	AlN, AlP, AlAs, AlSb, GaN, GaP, GaAs, GaSb, InN, InP, InAs, and InSb	Si and Ge	Cd_3P_2 and Cd_3As_2	Ag_2S and Ag_2Se	$CuInS_2$, $CuInSe_2$, $AgInS_2$ and $AgInSe_2$	CdHgTe

These substances all have band gap energies of less than 4.0 eV, making them semiconductors in both their bulk and QD forms. Table 2 gives the band gap energy for a few materials that are often used to make QDs. Both visible (380–750 nm) and near-infrared fluorescence wavelengths may be produced by choosing size and composition properly [17].

This thesis study mentions 3 types of QLEDs as semiconductor based InP QLEDs and CdSe QLEDs and carbon-based CQD LEDs in terms of material type [21].

Chapter 3

Quantum Dot Light Emitting Diodes

A type of semiconductor diode called a QLED (Light Emitting Diode) produces light when an electrical current or voltage is applied. With the applied current/voltage, motion occurs in electrons and holes in the device. Recombination occurs with the combination of electrons and holes directed towards each other. As a result of recombination, the energy of the electron is transformed into radiation of various colors in relation to the bandgap. They are called solid-state devices because the photon emission generated in the device is carried out by solid semiconductor material. A common nomenclature for both QLEDs (Quantum Dot LEDs) and OLEDs (Organic LEDs), this group differs from incandescent and tungsten halogen lamps (heated filaments) or fluorescent lamps (gas discharge) .

The color of the light emitted by the LED is due to the energy difference specific to the material, called the bandgap. This means that radiant materials with different bandgaps emit photons with different energies, so different colors of radiation are required.

3.1 Device Structure

Quantum Dot Light Emitting Diode (QLED or QDLED) is a semiconductor diode that emits light when electric current/voltage is applied. With the applied current/voltage, recombination occurs with the combination of electrons and holes directed towards each other. As a result of recombination, the energy difference of the electron is transformed into radiation of various colors in relation to the bandgap. This means that radiant

materials with different bandgaps emit photons with different energies, so different colors of radiation are required.

The frequently used structure of QLEDs is respectively; consists of anode, hole injection layer (HIL), hole transport layer (HTL), quantum dot layer (QD), electron transport layer (ETLs) and cathode (Figure 3.1) [22]. The materials used for these layers are optimized with the characterization results obtained and with the help of materials science.

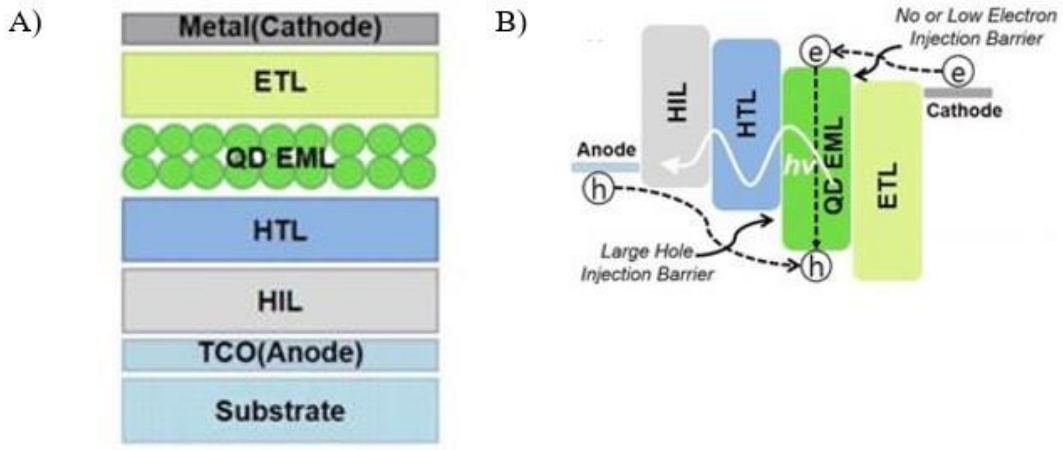

Figure 3.1 (A) QLED device architecture and (B) schematic of QLED working mechanism [22]**.**

3.2 Working Mechanism

Before explaining the working mechanism of quantum dot LEDs, the behavior of electrons should be mentioned. Two terms appear here: HOMO and LUMO.

HOMO is used as an abbreviation for “the highest occupied molecular orbital”. The one with the highest energy of the occupied molecular orbitals is called HOMO. LUMO, on the other hand, is known as “the lowest unoccupied molecular orbital”, and the one with the least energy of the unoccupied molecular orbitals is called LUMO. It is reported that the energies of HOMO and LUMO have an impact on the materials' electron affinities and ionization potential energies [23]. The lowest energy required to remove an electron

from the HOMO is the ionization potential energy, whereas the lowest energy required to add an electron to the LUMO is electron affinity [22].

The process for light emission and absorption is connected to the transformation of the electron's state. Its status depends on whether it is excited or not. The unexcited electron is in the ground state. The excited electron rises to the upper energy levels, but since it is not stable here, it tends to return to the ground state again. During this return, light is emitted due to the difference between the upper energy level and the ground energy level.

The basic working mechanism of quantum dot LEDs is as follows; A certain voltage (turn-on voltage or more) is applied to the device and the applied voltage difference creates electron (e^-) and hole (h^+) movement in the charge injection layers. Electrons and holes are injected correspondingly starting from the electrodes (anode and cathode) to the charge injection layer and then to the charge transport layers (CTL). The charge transport layers inject these carriers (e^- and h^+) into the quantum dot layer. The injected carriers initiate radiative recombination (radiation) in the quantum dot layer (Figure 3.1). The share of charge injection and conduction layers is high in the performance of QLEDs. It is of great importance that these layers, which also affect the device stability, have high carrier mobility, and can well balance the mutually occurring electron hole injections. Radiations formed outside the quantum dot layer emit different colors than QD in relation to the bandgap value of that layer, and this is an undesirable situation as it reduces the emitting quality of the device [24].

As mentioned in the previous section, QLEDs; It consists of hole transport, quantum dot and electron transport layers placed between the anode and the cathode. The sort of charge transport layer in the device (electrons or holes) can be used to categorize it. Since the classification criterion is determined according to whether the layers are organic or inorganic, 4 basic device types emerge (Figure 3.2) [25].

- Type-I) Organic/QD double layer
- Type-II) Organic-Organic charge carriers
- Type-III) Inorganic-Inorganic charge carriers

- Type-IV) Organic-Inorganic charge carriers

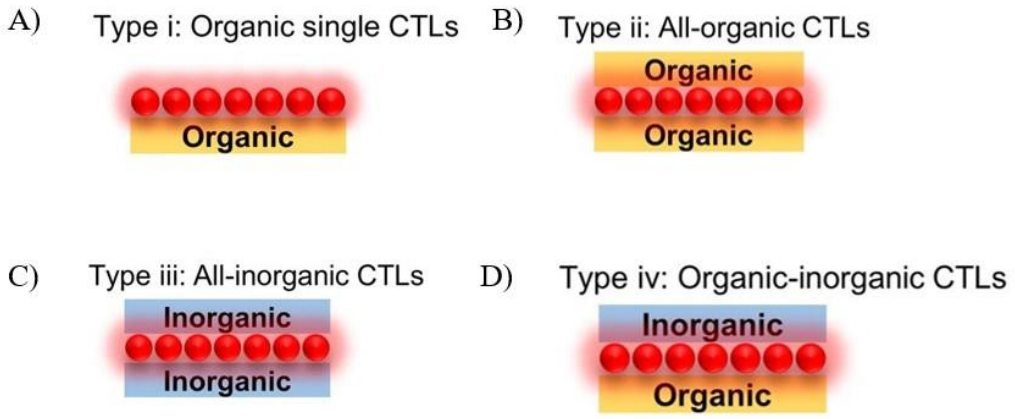

Figure 3.2 QLED classification by type of CTL [25]

Organic and inorganic materials are effective in the formation of the energy diagram of the device. The energy band values of these materials used in the device structure are shown in Figure 3.3. Materials such as PEDOT:PSS, PVK, Poly-TPD and TFB can be given as examples of organic materials [26]. Nickel Oxide (NiO), Molybdenum Trioxide (MoO_3), Vanadium Pentoxide (V_2O_5) and Tungsten Trioxide (WO_3), Zinc Oxide (ZnO), Tin (IV) Oxide (SnO_2), and Zinc Sulfide (ZnS) are examples of inorganic materials [27], [28].

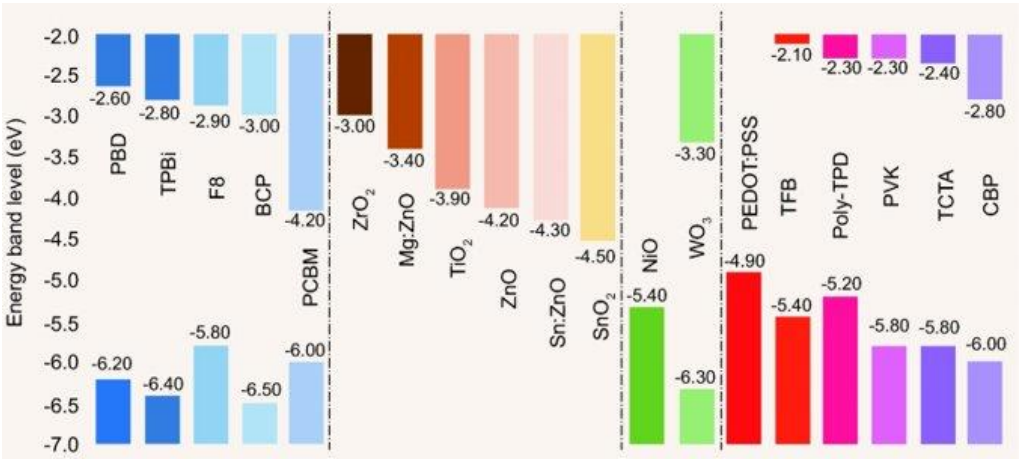

Figure 3.3 The energy-band levels of organic and inorganic charge transport layers [29]

3.2.1 Type-I) Organic/QD double layer

A thick layer of quantum dots serves as both the emission layer and the electron transport layer in the first QLED device. [30]. As Colvin et al [31] stated, a p-paraphenylene vinylene (PPV) and multi-layer cadmium selenide quantum dot (CdSe QD) structure was used. Due to its simplicity, organic/QD double-layer Type-I structure is common in the earliest QLEDs [32]. Besides, the electron injection control is poor and there is a leakage current problem. The maximum luminance obtained is about 100 cd/m^2 and the external quantum efficiency (EQE) is less than 0.01% [31]. This is due to the poor physical separation of the quantum dots and the charge transport layer, as well as the absence of the electron conduction layer (ETL) [24].

Then, by Dabbousi et al. (1995), quantum dots were disseminated into polyvinyl carbazole and an oxadiazole derivative [33]. In both early attempts, QD-LEDs with low turn-on voltage and impressive electroluminescence (EL) from polymers in addition to QDs were produced [34].

3.2.2 Type II: Purely organic charge carriers

To solve the problems observed in Type-I, Type-II device structure has been proposed [35]. A QD layer gets among an organic HTL and an organic ETL within the type-II structure.

A phase separation technique was created in 2002 by Coe et al [36]. This method, which relies on the creation of a single layer, is a tightly packed QD on a molecular organic hole transport layer.

A layer of organic molecules that were thermally evaporated ended the device structure. It had a low turn-on voltage, a little amount of emission from the organic layers, and an external quantum efficiency of around 0.52%. The Type-II device's peak EQE has been raised to 6% with this structure. Luminance is increased by 25 times over the previous best QLED results [35]. However, the fact that organic materials are very sensitive to moisture and oxygen causes the durability of Type-II devices to be low.

3.2.3 Type III: Completely inorganic charge carriers

Type III QLED structure is obtained by placing a quantum dot layer between two inorganic CTLs. Due to the high conductivity of inorganic materials compared to organic materials and their high resistance to oxygen and humidity, which are environmental factors, they constitute an important alternative for charge transport layers [25]. Considering these features, which are positive for QLEDs, completely inorganic charge carrier layers have been studied. In the first study, Mueller et al. (2005) sandwiched the quantum dot layers between p-type and n-type GaN. The EQE obtained here is less than 0.01% [37].

In subsequent studies, devices with inorganic-inorganic CTL's consisting of metal oxides have been demonstrated. In the studies of Caruge et al. [38] in 2008, a maximum brightness of 1950 cd/m^2 and a maximum external electroluminescence efficiency of approximately 0.1% were achieved, thus achieving 100 times improved performance compared to previous structures. According to Choi et al. [25], Type-III devices' long lifetime and superior stability at high current density hold potential for future flexible display applications. In their article, it is also mentioned that the quantum dots deteriorate under the coating conditions used for inorganic layers and thus the device performance decreases.

3.2.4 Type IV: Organic-inorganic charge carriers

Type-IV device structure consists of cargo transport layers, one organic and the other inorganic. Type IV, also known as hybrid structure, is generally found in a structure where the hole transport layer is organic, and the electron transport layer is inorganic. Therewithal the opposite structure is also heavily fabricated. While the advantage of organic materials is high gloss, the advantage of inorganic materials is their high stability [39]. To benefit from both organic and inorganic components, the hybrid structure was created [25].

In the first hybrid study by Caruge et. al. [40], the external quantum efficiency remained at 0.18% and their optoelectronic properties were close to type-III structures. In the ongoing studies, a significant increase was observed in the values with the addition

of ZnO (Zinc Oxide) nanoparticles to the Type-IV structure [24]. The main reasons for this rise are that ZnO nanoparticles have very good electron mobility and do not critically damage the quantum dot layer on which they are coated [41]. ZnO improves electron injection in the quantum dot layer. This improvement can be demonstrated by the low turn-on voltage of the LED and the reduction of photon emission occurring outside the quantum dot layer [24].

In addition, as Qian et al. (2011) [42] stated, it was observed that the stability of ZnO nanoparticles increased considerably with the addition of ZnO nanoparticles into the device architecture. In the article, it has been reported that the luminescence values of the devices reached a record level with 68,000 cd/m^2 (green quantum dot), with an initial brightness of 600 cd/m^2 and an operating life of more than 250 hours in low vacuum. Devices using ZnO nanoparticles as the electron conduction layer are very common due to their high electroluminescence (EL) values [43], and their potential application areas are wide due to the ultra-thin form factor suitable even for flexible displays. In the literature, 1.6×10^6 cd/m^2 luminance value has been achieved as a state of the art with structural optimizations in Type-IV devices and efficient syntheses in QD material [44].

Chapter 4

Experimental Methods

4.1 Material Synthesis

4.1.1 Zinc Oxide (ZnO) Synthesis

First, two distinct synthesis solutions were made: 0.1 M zinc acetate dihydrate solution in 30 mL dimethyl sulfoxide (DMSO) and 0.5 M tetramethylammonium hydroxide (TMAH) solution in 10 mL ethanol. The zinc solution was stirred for two minutes while the TMAH solution was progressively added. The stirring solution was then left for the reaction for an hour at ambient temperature. It was then progressively precipitated with acetone and acetone-hexane and dissolved into ethanol [45].

4.1.2 InP QD Synthesis

This part is taken from the article titled ‘’Tuning the Shades of Red Emission in InP/ZnSe/ZnS Nanocrystals for Fabrication of Light-Emitting Diodes’’ mentioned in Chapter 5.

The details of the synthesis processes have been summarized in Table 5.1 along with a schematic explanation in Figure 4.1. The method contains three steps core synthesis, HF injection, and shelling process. Typically, $InCl_3$, $ZnCl_2$, and OLA were mixed inside the glovebox (the amount of $InCl_3$ was 0.67 mmol). Then, the mixture was transferred to a 3-necked flask equipped with rubber septa and thermocouple and connected to the condenser. The mixture was degassed at 120°C for 30 min under vigorous stirring to completely dissolve the powders. Backfilled with N_2, it was heated to 180°C where 2.40 mmol 3DMA-P was quickly injected into the stirred solution and remained for desired reflux time (Step 1). Immediately after injection, the color of the

solution changed to red and dark red. Next, the reaction cooled down to 150 °C and after a short time heated again to 285°C. When it reached 170 °C, HF precursor and 1 mL of 1Se-TOP were injected (Step 2). Then, at 220 °C, 1.5 mL $ZnCl_2$-OLA and 4 mL ZnSt-ODE were co-injected. At 285°C, the reaction continued for 15 min. Then, 50 µL HF precursor, 1 mL of 2Se-Top, and 5 mL ZnSt-ODE were added, respectively, followed by stirring for 30 min. For the third and fourth ZnSe shells, 1mL 3Se-Top and 1 mL 4Se-Top were injected at 295°C (stirred for 30 min) and 305 °C (stirred for 60 min), respectively. In these steps, 6 mL ZnSt-ODE was also injected each time. To overcoat the QDs properly, the outer shell layers of ZnS were provided as follows. First, the reaction was heated to 310°C, and 1 mL S-TOP precursor was quickly injected followed by the addition of ZnOAc precursor and the reaction continued for an extra 45 min. Finally, the reaction was cooled down to 210°C and 0.6 mL of OT was dropwisely added and the reaction continued for 1 h (Step 3). In the end, the reaction rapidly cooled down to room temperature. To remove the unreacted species, hexane was added and centrifuged at 4000 rpm. The precipitated parts were discarded. Then, a suitable mixture of ethanol/acetone was added to the clear solution of QDs, to precipitate QDs, followed by centrifugation at 10000 rpm for 10 min. This process was repeated one more time, and the final purified samples were dried in the lab atmosphere. It should be noted that to make a reasonable change in shading the red emission (change in optical properties), we had to simultaneously modify several factors like what we did for RQ3 and RQ4: A decrease in reaction time (core synthesis) from 17 min to 12 min, and at the same time increase in $ZnCl_2$ amount (from 3.3 mmol to 3.87 mmol) (Table 5.1).

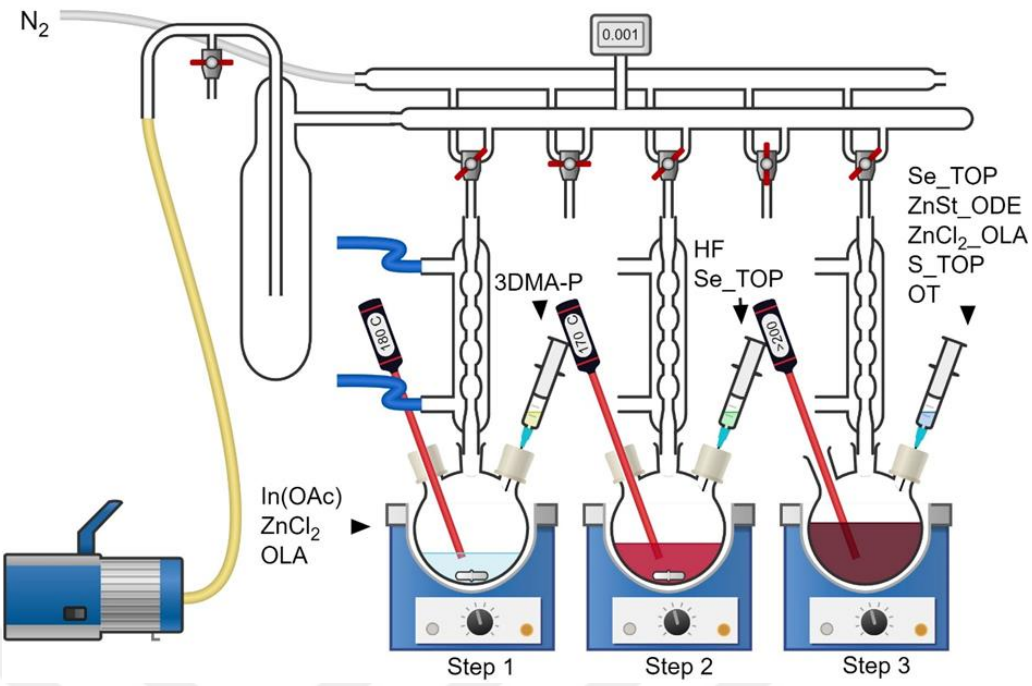

Figure 4.1 Schematic illustration of the synthesis method used for the preparation of InP/ZnSe/ZnS QDs.

4.1.3 Carbon QD Synthesis

This part is taken from the article titled '' Spectrally Tunable White-Light-Emitting Diodes Based on Carbon Quantum Dot-Doped Poly(N-vinylcarbazole) Composites'' mentioned in Chapter 6.

A solvothermal method was used for the preparation of high-quality CQDs. 1 mmol of citric acid and 0.5 mmol of urea were added into 30 mL toluene and heated at 40 °C for a short time. Then, 0.5 mmol n-octylamine was added into the mixture which was again stirred for a while. After that, it was transferred to a 100 mL Teflon-lined autoclave and reacted at 205 °C for 14 h. Finally, the reactor was put outside of the oven and left to cool down naturally. To purify the colloidal product, the as-prepared colloidal CQDs were first centrifuged at 10000 rpm for 10 minutes to discard the unreacted species and then filtered by a 0.22 um polytetrafluoroethylene (PTFE) filter. In the next step, using the silica-gel column chromatography as stable phase and dichloromethane (DCM) / methanol as eluent mobile phase, purified CQDs with strong yellow emission were

separated. In the end, it was concentrated via a rotary evaporator and redispersed in DCM for further experiments and device fabrication. A schematic illustration of synthesis method and possible structure of CQDs have been drawn in Figure 4.2.

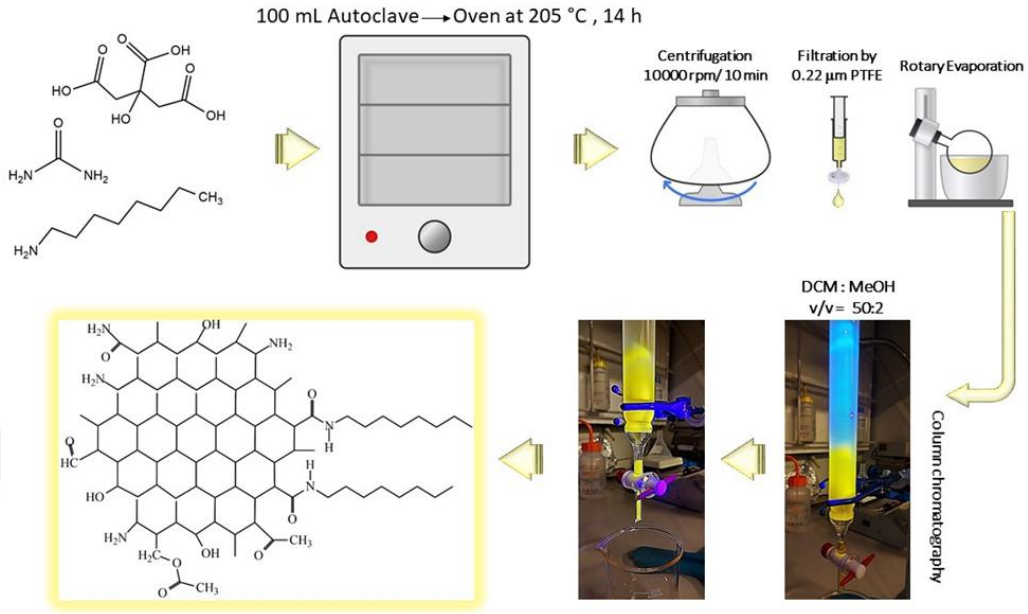

Figure 4.2 Schematic of synthesis method and formation mechanism of CQDs

4.1.4 CdSe/ZnS QD Synthesis

0.3 mmol of cadmium oxide (CdO), 4 mmol of zinc acetate (Zn-Ac) and 5 mL of Oleic Acid (OA) are placed in a 50 mL flask and placed in a magnetic stirrer with heating. The solution is heated to 70°C under argon gas. Vacuum is applied for 20 minutes, during which the temperature is increased to 135° C under vacuum, allowing the materials to dissolve in OA. After the temperature is lowered to 95°C, 15 mL of 1-Octadecene (ODE) is added to the system, and oxygen and moisture are removed by applying vacuum for 1 hour at this temperature. The system is heated to 300°C in an argon inert environment. It is prepared by dissolving 0.3 mmol Selenium (Se) and 3 mmol sulfur (S) into 2 mL Trioctylphosphine (TOP), which will be used to form nuclei of quantum dots by rapid injection at high temperature, in an Argon inert glovebox medium. In order to ensure a homogeneous size distribution, the solution is quickly injected into the system by increasing the mixing speed. At this temperature, it is waited for 10 minutes for the formation and growth of quantum dots. The resulting quantum dots turn the solution into

an orange and greenish color, respectively. After waiting, the system is cooled down to room temperature and the synthesis ends. 15 mL of n-hexane is added to ~25 ml of product placed in the centrifuge tube and precipitation is applied for 10 minutes at 5000 rpm. In this way, unreacted chemicals and unstable materials precipitate. The remaining liquid is separated into a separate tube. Acetone and 6 mL of methyl alcohol are added at a ratio of 1:1 to the quantum dots in n-hexane colloidally and centrifuged at 5000 rpm for 10 minutes. The liquid that accumulates on the top is separated, the precipitated quantum dots are dispersed in n-hexane, characterization processes are performed and stored at +4 °C [46].

4.2 Fabrication

The QLED fabrication phase can be explained in 6 basic steps. Although these steps and the materials used may vary, the commonly applied processes can be listed as follows.

I. Preparation of the anode layer

II. Preparation of substrates

III. Coating of hole injection-transmission layers

IV. Coating of the emissive layer

V. Coating of electron injection-conduction layers

VI. Coating of the cathode layer

4.2.1 Preparation of the anode layer

The first step of QLED fabrication begins with the selection of the LED base/substrate. Generally, glass or pet bases are used because they are transparent. The high transparency of the selected base is important as it will allow more of the emitted light to go out of the LED and affects the measurement results. Then the layer that will serve as the anode is coated on the substrate.

As transparent conductive oxides, FTO (Fluorine-doped Tin Oxide), AZO (aluminum-doped zinc oxide), ITO (indium tin oxide) [47], metal mesh (Metal Mesh) [48], PMA-Au-PMA (phosphomolybdic acid-gold-phosphomolybdic) as anode acid) [49], silver nanowires (Ag NWs) [50] and carbon nanotubes can be used.

In addition to the unique properties of each material, ITO is mostly used in QLEDs. The reason for using ITO is that it has low electrical resistance ($2x10^{-4}\Omega$-cm) [51] as well as high carrier concentration. Also, ITOs have a commonly used work function of ~ 4.7 eV (4.1-5.3 eV [52], [53] and high light transmittance (>85%) [51] in the visible range. ITO plays a crucial role in device performance because it influences the height of the energy barrier at the heterojunction interface [54]. Due to these high electrical and optical properties, it finds potential applications in many fields such as flat panel displays, solar cells, gas sensors, cameras, anti-reflective coatings, heat reflecting mirrors, and surface heaters for automobile windows. [55]. The substrates we used in our work have the size of 15 mm x 20 mm and coated with ITO as the anode layer. Each substrate consists of 6 pixels, each pixel has an active area of 4.5 mm^2 (Figure 4.3), which can glow when electric current is applied. Although patterns can be created in laboratories, substrates are purchased ready-made to increase homogeneity. In this way, time can be saved by starting directly with step II during fabrication.

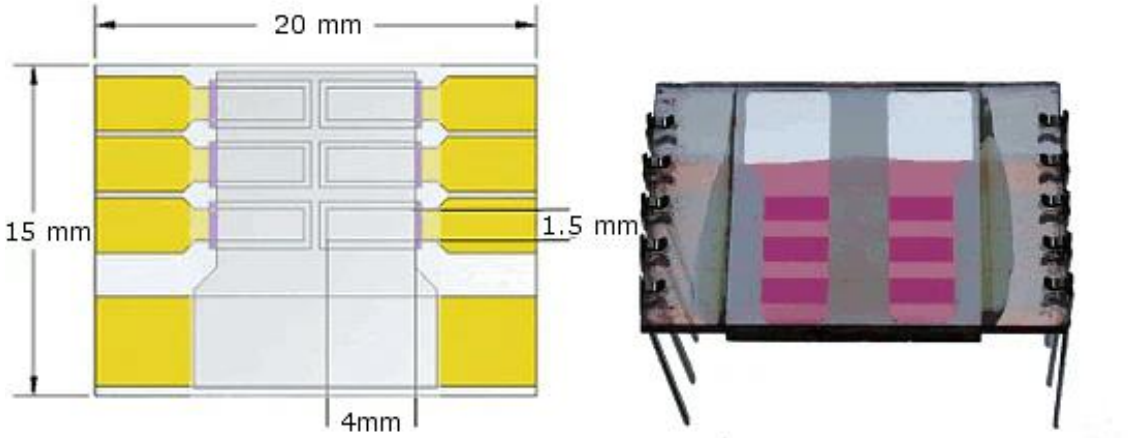

Figure 4.3 QLED substrate – patterned ITO coated glass [56]

4.2.2 Preparation of Substrates

The second step in fabrication is the preparation of substrates. This stage is also called the cleaning stage. Substrates are subjected to certain processes to be purified from possible impurities on them.

The layer thicknesses of QLEDs are mostly in the nanometer scale (<100 nm) [57]. Considering that dust particles or chemical residues from very small structures can be found on the glass substrate, they may be larger than the total thickness of the device layers. Even if their size is small, these unwanted impurities increase the surface roughness considerably and are likely to reduce the operating performance of the LED. On the other hand, the coating on a well-cleaned substrate adheres better to the surface and increases the homogeneity of the layers on the device surface.

Cleaning begins by adding 0.1% by volume Hellmanex III to the hot deionized water (approximately 100°C) in the beaker. Then, each beaker is sonicated for 7 minutes by being taken to an ultrasonic cleaner that provides good cleaning with high-frequency sound waves. The sonication process is repeated with hot deionized water and isopropyl alcohol, respectively, and the substrates are dried with nitrogen gas. The dried substrates are kept in the plasma cleaner for 10 minutes to clean the sample surface and improve the wetting properties by making surface functionalization. This method can provide nearly atomically clean surfaces without damaging the sample.

4.2.3 Fabrication of Devices

Gloveboxes are enclosed environments where HIL, HTL, EML, and ETL materials are coated, and following procedures are carried out. Glovebox is a special system in which there is a high percentage of inert gas (or nitrogen), the amount of oxygen and water vapor is kept under control, and the gas pressure is constantly balanced. The reason why the processes are carried out in the glovebox is to minimize or eliminate the interaction of the materials used and the gases in the environment. Inert gases and nitrogen are used in the system as they do not react with most substances [58]. The interactions to be reduced in the glovebox are usually oxidation from oxygen or hydrolysis from water

vapor. PEDOT:PSS used as HIL and in aqueous solution is the exception of the above materials and is coated outside the glovebox [59].

Coating of the solution form layers of QLEDs is done in the spin coating device. The spin coater is effective in determining the thickness of the layer and uniform coating. Then, the solid layer form is formed by annealing on the hot plate at a temperature suitable for the solvent of the layer solution.

Some organic materials in powder form are coated in the organic evaporator, and the cathode layer, usually aluminum, is coated in the metal evaporator. These two systems in the thermal evaporator are carried out in vacuum at a pressure of 10^{-7} torr, by heating the melting pot and masking. The materials are coated in the planned areas in the form of vapor and then solidified on the surface to form a solid layer.

Although the coating of the cathode layer is sufficient for the device to operate, devices taken outside the glovebox for characterization interact with gases in the air. With the exception of gold, the majority of metals oxidize when they are exposed to air and water. After a while, this reaction, which makes silver dull and iron rust, can weaken the metal and create fissures or structural problems [60]. This interaction has disruptive effects on metals such as aluminum and silver, which are used as cathodes, and therefore on QLEDs.

4.2.4 Encapsulation of Devices

To prevent degradation, a conservation process called encapsulation is performed. In addition to the protective effect of encapsulation, studies have also shown that it has an effect that increases QLED efficiency and luminance over time, also known as positive aging [61]-[62]. The encapsulation process is performed by dripping epoxy on the last coated cathode layer, putting glass on it, and then exposing the devices to ultraviolet light for a certain time. During the ultraviolet treatment, the epoxy hardens, bonding the substrate and the encapsulation glass together. In this way, the contact of the cathode layer with the atmosphere is cut off. Figure 4.4 (A) shows the photo while QLED devices are encapsulating in our laboratory and (B) shows the one of that devices which are encapsulated with epoxy and glass.

A) 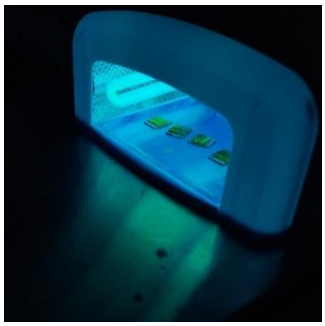 B) 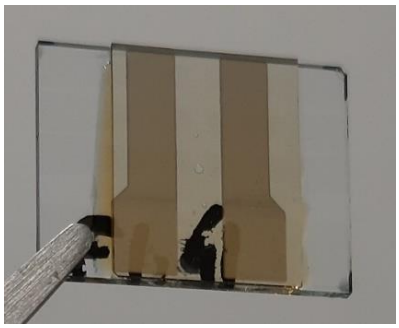

Figure 4.4 (A) The UV cabinet used in the encapsulation process (B) An encapsulated QLED device.

4.3 Characterization

For our characterization studies of QLEDs, Hamamatsu Photonic Multichannel Analyzer, Keithley 2400 Power Supply-Multimeter Unit, integrating sphere, and Scanning Transmission Electron Microscope (STEM) devices were used in our laboratories (Figure 4.5). In these devices, many parameters such as voltage, current, current density, and time interval to be applied during the operation can be adjusted. Using these parameters, graphs are created with measurements such as EL spectrum-wavelength, luminescence-voltage, luminous flux, external quantum efficiency-voltage and current efficiency. With the electron microscope method, both the structures of the coated films and the morphological properties of the nanoparticles are examined.

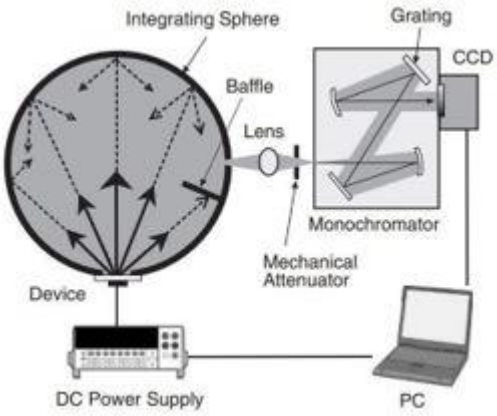

Figure 4.5 A integrating sphere and a very sensitive CCD spectrum analyzer for optically analyzing QLEDs. [63]

4.3.1 Luminance (L)

The emission of electromagnetic radiation in the visual range by matter in general is referred to as luminosity or luminescence. It is a photometric measurement that may be used to describe light sources, as well as the light that is reflected or that flows through an area in particular [64]. It is used to determine how glossy a surface is [65]. The photopic eye response curve's action spectrum illustrates how humans respond to light (Figure 4.6), influences the lumen, which quantifies the produced quantity of light sensible to human eye produced [66]. It is determined by multiplying the sensitivity function of the eye (Figure 4.6) by the intensity of light from the visible spectrum per unit area (m^2) traveling in a certain direction.

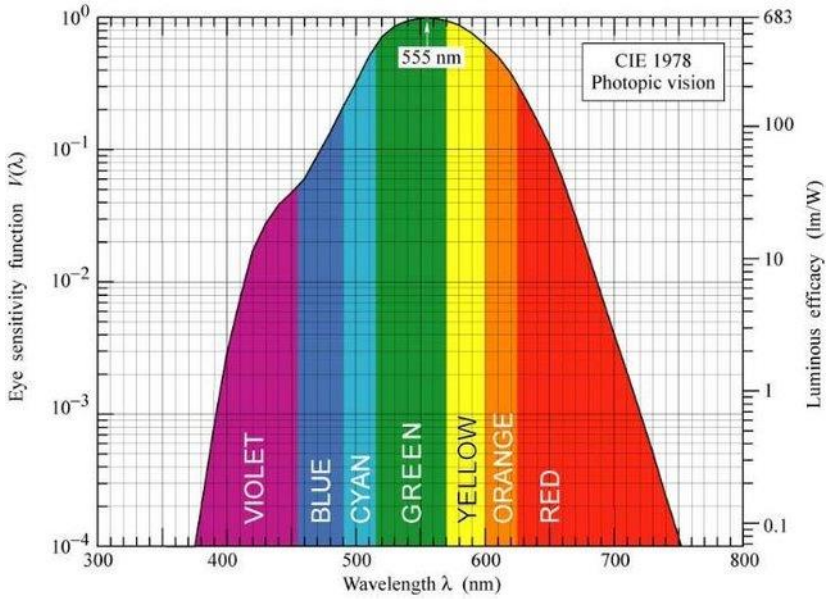

Figure 4.6 Human Eye Sensitivity Function

$$L = 683 \frac{lm}{W_{\mathbf{opt}}} \int \mathrm{P_L}(\lambda) V(\lambda) V(\lambda) \tag{4.1}$$

This luminance (L) is expressed in cd/m^2 (candela/square meter) in the SI (International System of Units) unit system. However, nit, which is equal to 1 cd/m^2, is another luminance unit.

If the device is exposed to a sufficiently intense light source, that is, by photon absorption, it is called photoluminescence, and if it is formed by the applied electrical current, it is called electroluminescence. This thesis study covers electroluminescent devices.

4.3.2 External Quantum Efficiency (EQE)

The photon emission efficiency of the LED is represented by the external quantum efficiency value, abbreviated as EQE, and expressed as a percentage. It can be expressed as the ratio of the total amount of photons emitted by the LED to the total number of charge carriers that flow through the device. In other words, it means how efficiently the device converts electrons and holes into photons and how effectively these photons are emitted from the device. Equation below shows total absolute emission intensity (λ and Ω are wavelength and solid angle, respectively):

$$\int \mathbf{F_{abs}}(\boldsymbol{\lambda}, \boldsymbol{\Omega})\mathbf{d\Omega d\lambda} \tag{4.2}$$

$$\eta_{\mathbf{ext}} = \frac{\iint \frac{\mathbf{F_{abs}}(\boldsymbol{\lambda},\boldsymbol{\Omega})}{\mathbf{hc}/\boldsymbol{\lambda}} \mathbf{d\Omega d\lambda}}{\boldsymbol{J}/\mathbf{e}} = \frac{\mathbf{N_p}}{\mathbf{N_e}} \tag{4.3}$$

Here, c represents the speed of light, h the Planck constant, I value is operating current and e is charge of electron, N_p is number of photons emitted, and N_e is number of charge carriers injected [63]. Total absolute emission intensity gives electroluminescent intensity for all solid angle and wavelength. The total number of photons is found by dividing this by the energy of a single photon and integrating it across all wavelengths. In the divisor part, the total number of injected electrons is found by dividing the current by the electron charge. Basically, EQE is found by the ratio of these two. This calculation can be done with systems developed for precise measurements using an integrating sphere and spectrometer.

Chapter 5

Indium Phosphide QLEDs

The following part has been compiled by taking the relevant parts of QLED from the article titled “Tuning the Shades of Red Emission in InP/ZnSe/ZnS Nanocrystals for Fabrication of Light-Emitting Diodes”. This article has been submitted to a journal for publication and in the review stage.

Tuning the Shades of Red Emission in InP/ZnSe/ZnS Nanocrystals for Fabrication of Light-Emitting Diodes

Ehsan Soheyli[1]*, Aysenur Arslan[1], Sultan Suleyman Ozel[1], Kevser Sahin Tiras[2], Evren Mutlugun[1]*

1 Department of Electrical-Electronics Engineering, Abdullah Gul University, Kayseri 38080, Türkiye

2 Department of Physics, Faculty of Sciences, Erciyes University, Kayseri 38030, Türkiye

5.1 Abstract

While Cd-based luminescent nanocrystals (NCs) are the most mature NCs for fabricating an efficient red light-emitting diode (LED), the toxicity-related limitation is their inevitable property, making it necessary to find a promising alternative. From this point of view, multi-shell coated red-emissive InP-based NCs are excellent luminescent nanomaterials to be employed as an emissive layer in electroluminescent (EL) devices. However, due to the presence of oxidation states, they suffer from a wide emission spectrum, limiting their performance. This study uses tris(dimethylamino)phosphine

(3DMA-P) as a low-cost aminophosphine precursor and a double HF treatment to present a cost-effective, one-pot, up-scaled hot-injection synthesis of purely red emissive InP-based NCs. The InP core structures were coated with thick shell layers of ZnSe and ZnS to prevent charge delocalization and create a narrow size distribution. Therefore, purified NCs showed an intense emission signal as narrow as 43 nm across the entire red wavelengths (626-670 nm) with emission quantum efficiencies of 74% at 632 nm and 60% for far-red wavelengths of 670 nm which are one of the best results (especially the deep-red wavelength) among one-pot colloidal methods reported yet for red-emissive InP-based NCs. Samples showed a relatively long average emission lifetime of 50-70 ns with a biexponential decay profile. To demonstrate the practical ability of the prepared NCs in optoelectronics, we fabricated red-emissive InP-based LEDs. The device showed an external quantum efficiency (EQE) of 1.16%, a luminance of 1039 cd.m-2, and current efficiency of 0.88 cd.A-1.

5.2 QLED Fabrication

Glass substrates pre-coated with ITO were cleaned in an ultrasonic cleaner using a mixture of soap and hot DI water, hot DI water, and isopropyl alcohol, respectively, for 10 minutes each. This was followed by drying the substrates with nitrogen and plasma cleaning. On top of ITO substrates, filtered PEDOT:PSS as an efficient hole injection layer was spin-coated at 3500 rpm for 3 s and 5000 rpm for 57 s. After that, they were annealed at 150 °C for 30 min. Then, the substrates were transferred into the glove box. The hole transport layer was spin-coated using a 6 mg/mL chloroform solution of PVK on PEDOT:PSS-coated substrates at 3000 rpm for 60 s and annealed at 150 °C for 30 min. InP/ZnSe/ZnS QDs (10 mg/mL in hexane) were dynamically spin-coated on the PVK layer at 1250 rpm for 30 s as an emissive layer. For the electron transport layer, 20 mg/mL ZnO solution was spin-coated at 2000 rpm for 60 s and annealed at 90 °C for 30 min. To complete the device fabrication, Al (100 nm) was thermally evaporated as the cathode layer at a base pressure of 5×10^{-6} Torr. Before the devices were taken out for characterization they were encapsulated with UV-curable epoxy and encapsulation glass.

5.3 Characterizations

A set of characterization techniques was used to evaluate the structural and optical properties of the purified InP/ZnSeS/ZnS QDs, and to measure the optoelectronic characteristics of the fabricated QLEDs. In this regard, XRD pattern (Bruker D8 Discover), STEM/EDX (Thermo Fisher Scientific equipped via ELECT plus detector and Gemini 300 microscope), FT-IR (NICOLET 6700), UV-Vis (Thermo Genesys 10S), PL (Cary Eclipse), TRPL (PicoQuant Fluo Time 200 time-correlated single photon counting system) spectra, and PLQE measurements (Quantaurus-QY instrument- Hamamatsu) were performed to analyze the purified QDs. The luminance, EQE, current density, and electroluminescence (EL) characteristics of devices were measured by using Hamamatsu PMA-12 photonic multichannel analyzer and Keithley 2400 source meter together with an integrating sphere.

5.4 Results and Discussion

The optical characteristics of the purified InP/ZnSe/ZnS QDs have been evaluated using a set of measurements to demonstrate the optical advantages of these QDs. While the synthesis process is one-pot, without performing a separate purification of the core QDs, the UV-Vis spectra of all samples showed two absorption peaks proving the well-resolved and appropriate electronic structure of the prepared QDs (Figure 5.1A).

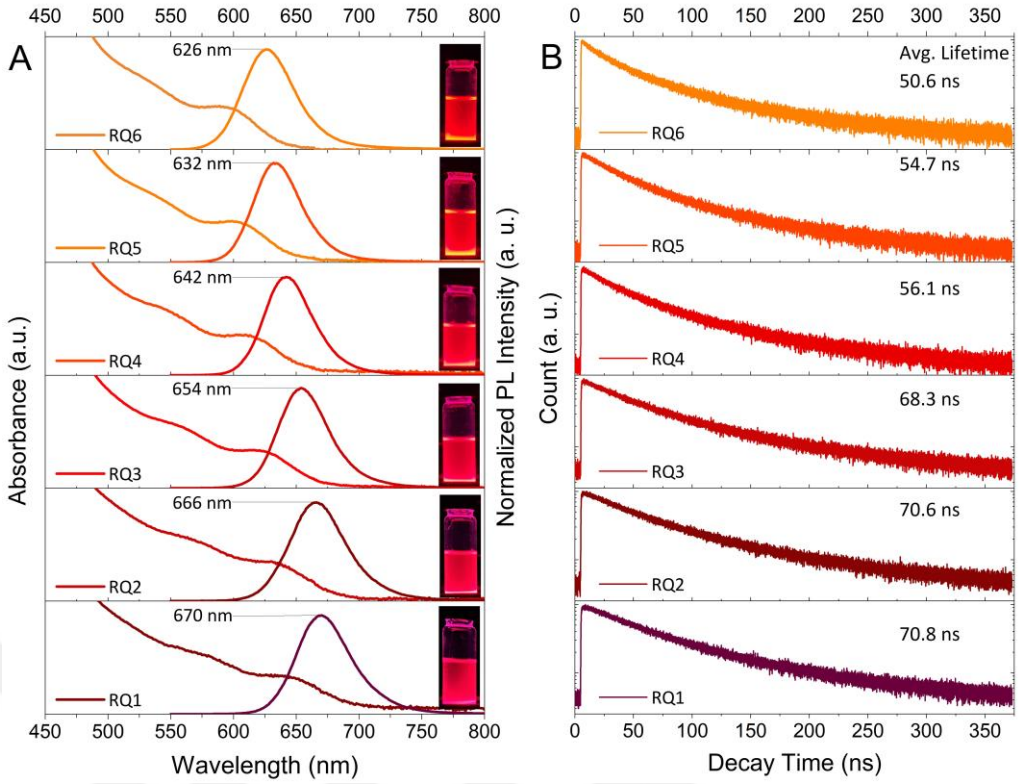

Figure 5.1 A) UV-Vis and PL spectra of purified InP/ZnSe/ZnS QDs (Inset shows digital images of purified QDs dispersed in hexane, under 365 nm UV lamp). B) TRPL profiles of the corresponding QDs.

It also confirms a blue shift in the first absorption peak from 645 nm (RQ1) to 595 nm (RQ6), upon changing the experimental parameters (Figure 5.1A and Table 5.1).

Table 5.1 : Details of the experimental parameter used to change the optical properties of the purified InP/ZnSe/ZnS QDs.

Code	$InCl_3$ (mmol)	$ZnCl_2$ (mmol)	OLA (mmol)	T_R (min)	HF-Acetone (uL) Temp. of Injection (°C)	UV/ PL Position (nm)	PLQE (%)	FWHM (nm)
RQ1	0.67	3.3	3.04	20	0	642 / 670	60	50
RQ2	0.67	3.3	3.04	20	60/ 270	631 / 666	66	52
RQ3	0.67	3.3	3.34	17	[1]170/170 [2]50/ 285	621 / 654	68	47
RQ4	0.67	3.87	3.34	12	[1]170/170 [2]50/ 285	611 / 642	71	45
RQ5	0.67	3.87	3.52	8	[1]170/170 [2]50/ 285	601 / 632	74	44
RQ6	0.67	4.34	3.34	5	[1]170/170 [2]50/ 285	592 / 626	69	49

Simultaneously, the PL emission spectrum experiences a blue shift from 670 nm (RQ1) to 626 nm (RQ6), fully covering the red region of the visible spectrum. In addition

to the emission wavelength, the full width of the PL profiles of the prepared QDs is also in an excellent range as narrow as 44 nm for the RQ5 sample with PL peak located around 632 nm. In all cases, the Stocks shift is around 30 nm (between 28-34 nm for all samples), which shows the main role of excitonic states in the recombination of excited carriers, and it works for all samples. Interestingly, while the PL peak position was located in a wide range, the FWHM was reasonably narrow (50 nm) even for the RQ1 sample with PL emission located at a far-red region of 670 nm. As shown in Table 1, the recorded FWHM values of PL emission spectra for all the samples were 44-52 nm which are excellent results for such a one-pot approach. In the method employed here, the thick shell of ZnSe not only decreases the possibility of exciton leakage toward the surface of the QDs but also shifts the bandgap to longer wavelengths, facilitating access to the deep-red region. Such a multi-layer structure is also beneficial to decrease the size distribution and improve the emission purity. To further demonstrate the high-red-color purity of the emission, digital images of the purified QDs redispersed in hexane have been captured under 365 nm irradiation (Inset of Figure 5.1A). Independent of the emission wavelength, all QDs show a pure red color emission.

The PLQE of all samples was measured by absolute method at the excitation wavelength of 320 nm. As mentioned in Table 5.1 the highest PLQE is 74% for RQ2 and it preserves up to 60% even at long emission wavelengths of >665 nm. This can be considered as strong evidence for the functionality of the prepared QDs for the fabrication of red-emissive required systems. To evaluate the number of energy levels contributing to the recombination of excited charge carriers, time-resolved photoluminescence (TRPL) measurements were performed via a time-correlated single photon counting (TCSPC) system. As shown in Figure 5.1B and confirmed via exponential fitting of each profile (Table 5.2) there are two radiation pathways, including fast and slow decay components, indicated with shorter (τ_1) and longer (τ_2) lifetimes. The shorter component is related to the recombination centers commonly known as midgap-energy levels, while the longer one is due to the excitonic states involving radiative emissions. Interestingly, the latter component shows a long lifetime of up to 125 ns. The calculated average lifetimes of the RQ1-to-RQ6 are 70.8, 70.6, 68.3, 56.1, 54.7, and 50.6 ns, respectively. This alteration indicated that upon blue-shift in the PL peak position, the average lifetime decreases

which can be attributed to an increase in the bandgap energy and a more dominant contribution of localized energy levels in the bandgap.

Table 5.2 Table 5.2 The lifetime components of the InP/ZnSe/ZnS QDs

QDs Code	RQ1 (670 nm)	RQ2	RQ3	RQ4	RQ5	RQ6 (626 nm)
τ_1 (ns)	45.0	46.6	40.0	31.3	32.2	25.1
A_1 (Counts)	634.0 ± 16.0	580.8 ± 15.4	539.2 ± 16.9	524.6 ± 7.8	596.4 ± 19.1	500.1 ± 21.6
τ_2 (ns)	125.1	115.0	112.6	94.2	96.5	85.5
A_2 (Counts)	301.1 ± 6.9	314.3 ± 7.3	344.4 ± 7.4	342.3 ± 7.8	321.6 ± 7.8	365.7 ± 8.3
τ_{avg} (ns)	70.8	70.6	68.3	56.1	54.7	50.6
χ^2	0.991	0.990	0.996	1.020	1.002	1.001

Here using these InP/ZnSe/ZnS QDs (RQ5), we fabricated QLEDs comprising ITO/PEDOT:PSS/PVK/QDs/ZnO/Al. The device configuration is shown in Figure 5.2A. In Figure 5.2B, the current density-voltage-luminance (J-V-L) characteristics of the QLED shows that when the voltage is 12 V, the maximum brightness is 1039 cd/m^2 and the current density is 465.5 mA.cm^{-2}. The turn-on voltages of QLED were around 5 V. Figure 5.2C shows the change in the external quantum efficiency (EQE) versus the brightness. As the EQE is at its maximum value of 1.16%, the brightness is 50.64 cd/m^2. When the brightness reaches its maximum value at 1039 cd/m^2, the EQE is 0.29%. Figure 5.2D gives the change in the EQE as the driving voltage is increasing, and the maximum

EQE reaches up to 1.16% at 6.6 V. As illustrated in Figure 5.2E with an image of the device taken at a driving voltage of 13 V as the inset, EL intensity peaks at 640 nm at a driving voltage of 12.6 V. Figure 5.2F shows that CIE x-y coordinates (0.69-0.30) are located in the deep red region. It has been postulated that electron transport, which is influenced by the QDs layers and shell thickness, is more important for determining the total current density [67]. Furthermore, the EQE and luminescence of the LEDs were vastly affected by our thick ZnSe interlayer thickness. As previously found, a thick shell for Cd-based QDs helped prevent Auger recombination, which results in QDs charging and a decrease in device efficiency [68]. The inter-particle distance can be increased and the energy transmission between nearby QDs can be decreased by a thick shell [69].

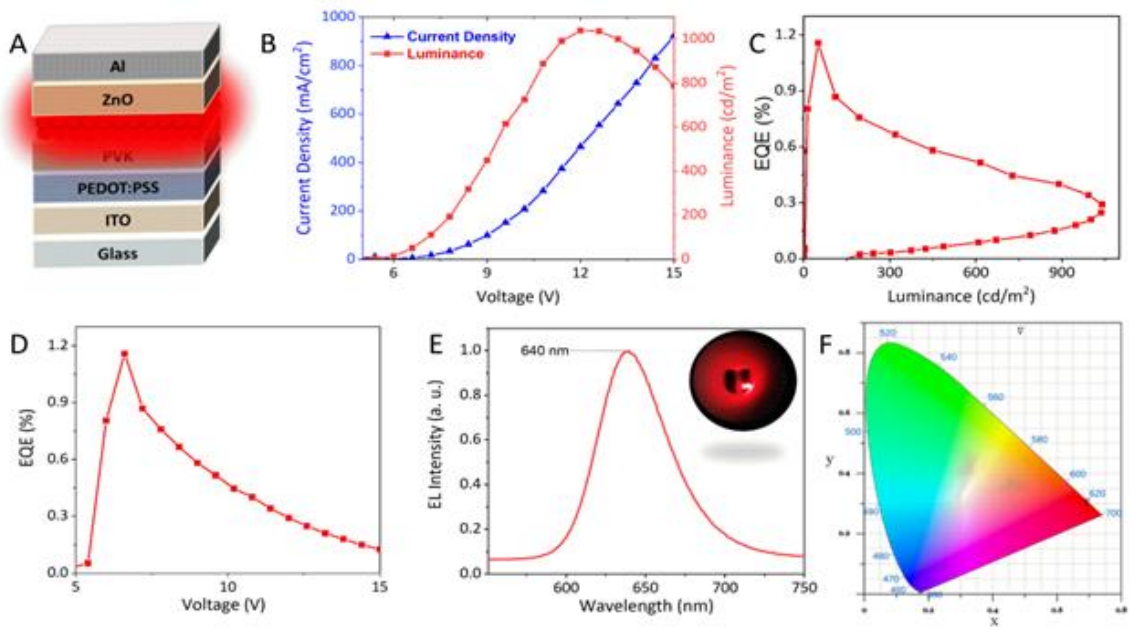

Figure 5.2 A) QLED device configuration. B) The J–V–L curve of the QLED. EQE versus C) Luminance and D) Voltage. E) The QLED's EL spectra and a photograph of the LED at 13 V in running. F) CIE coordinates of the QLED

5.5 Conclusion

The demand for the fabrication of efficient QLEDs with high-quality, stable, and less-toxic QDs is at the heart of current research in optoelectronic devices. The present study suggested a facile one-pot colloidal method to prepare high-quality InP-based QDs

with narrow emission within the red region of the visible spectrum. In summary, InP/ZnSe/ZnS QDs were synthesized by using HF-assisted surface fluorination and implementing a thick mid-shell layer of ZnSe at high temperatures. Upon the change in experimental parameters, QDs covered all the red regions of the visible spectrum from 626-670 nm, with the highest PLQE of 74%, and narrow FWHM of 43 nm. They also demonstrated a PLQE of more than 60% for far-red emission wavelengths. To confirm the capability of these QDs in practical luminescent devices, a QLED was fabricated using InP-based QDs as the emissive layer. Results showed a maximum EQE of 1.16% and brightness of 1039 cd/m^2 at 640 nm which is typically located at longer wavelengths concerning the other reports.

Chapter 6

Carbon QD LEDs

The following part has been compiled by taking the relevant parts of QLED from the article titled “Spectrally Tunable White-Light-Emitting Diodes Based on Carbon Quantum Dot-Doped Poly(N-vinylcarbazole) Composites”. This article has been submitted to a journal for publication and in the review stage.

Spectrally Tunable White-Light-Emitting Diodes Based on Carbon Quantum Dot-Doped Poly(N-vinylcarbazole) Composites

Kevser Sahin Tiras[1], Aysenur Arslan[2], Ehsan Soheyli[2]*, Evren Mutlugun[2]*

1 Department of Physics, Faculty of Sciences, Erciyes University, Kayseri 38030, Türkiye

2 Department of Electrical-Electronics Engineering, Abdullah Gul University, Kayseri 38080, Türkiye

6.1 Abstract

Electroluminescent white light-emitting diodes (WLED) are always of great interest for emerging display applications. Carbon-based quantum dots (CQDs) are the newest emerging nanoscale materials that can be employed for this purpose, owing to their broad and bright light emission properties. In the present work, highly luminescent CQDs with an emission quantum yield of 60% were prepared via the colloidal solvothermal method

and subsequent silica gel column chromatography. The photoluminescence (PL) peak was located at 550 nm possessing yellow emission, with full-width at half maximum of 98 nm and a relatively long lifetime of 10.23 ns through a single-exponential recombination pathway. CQDs were employed in an electroluminescent device architecture of ITO / PEDOT:PSS / TFB / PVK:CQD / TPBI / LiF / Al structure and blended with poly(N-vinyl carbazole) (PVK) to evaluate their ability to reach white electroluminescent emission. Results confirmed a high external quantum efficiency (EQE) of 0.76% and maximum luminescence of 774.3 cd.m-2. Tuning the ratio between CQDs and PVK from 1:10.25 to 1:5.75 resulted in a systematic shift in CIE x-y coordinates from 0.23-0.26 to 0.21-0.24, located close to the cool white region. The results of the present study can be considered a step forward in fabricating efficient WLEDs based on low-cost CQDs.

6.2 CQD-LED Fabrication

Glass substrates pre-patterned with indium tin oxide (ITO) were cleaned in an ultrasonic cleaner to remove impurities by using a 0.1% volume ratio Hellmanex: hot DI water mixture, hot DI water, and isopropyl followed by plasma cleaning. As the hole injection layer PEDOT:PSS was spin-coated on ITO at 5000 rpm for 60 s, then annealed at 150°C for 20 min. After annealing, substrates were transferred into the argon-filled glove box. Then, 8 mg/mL chlorobenzene solution of TFB was spin-coated on the PEDOT:PSS layer at 3000 rpm for 60 s and annealed at 150°C for 30 min. CQDs (15 mg/mL in DCM) doped in 6 mg/mL PVK solution in chloroform. The blends were prepared in different volume ratios of CQD and PVK to use as an emissive layer. By keeping the total volume of all the blends the same only CQD:PVK volume ratios changed and the ratios follow as 1:5.75, 1:7.25, 1:8.75, and 1:10.25. CQD-PVK solutions were spin-coated on TFB at 2000 rpm for 60 s and annealed at 60°C for 15 min. The cathode layer consisting of LiF and Al was deposited by thermal evaporation at a base pressure of 5×10^{-6} Torr on top of thermally evaporated 70 nm of electron transport layer TPBi. Finally, to protect the device from oxidation and humidity the active area of the device was encapsulated with UV-curable epoxy and encapsulation glass.

6.3 Characterizations

The X-ray diffraction (XRD) pattern was collected via Bruker D8 Discover. The attenuated total reflectance (ATR) Fourier transform infrared (FTIR) spectroscopy known as ATR-FTIR was performed using the FT-IR spectroscopy model NICOLET 6700 made by a Thermo-scientific company. The EDX elemental analysis was performed by Thermo Fisher Scientific equipped via ELECT plus detector and Gemini 300 microscope. Transmission electron microscopy (TEM) has been performed via . The optical spectroscopies were performed via UV-Vis, PL/PL excitation (PLE), time-resolved PL (TRPL) spectroscopies, and measurement of PLQY. Data were recorded using Thermo Genesys 10S spectrometer, Cary Eclipse, PicoQuant Fluo Time 200 time-correlated single photon counting system (TCSPC), and Quantaurus-QY instrument made by Hamamatsu company, respectively. Hamamatsu PMA-12 photonic multichannel analyzer and Keithley 2400 source meter together with integrating sphere were used for characterization. The luminance, EL, and color coordinates values of the devices have been tested with these instruments.

6.4 Results and Discussion

As a main physical property of a nanomaterial that determines the capability of being used in LEDs, the optical properties of the purified CQDs were evaluated. Figure 6.1A shows the UV-Vis, PLE, and PL spectra. The absorption spectrum showed an obvious absorption peak located at 437 nm attributed to the C=O bonds (due to surface C=O functional groups), whose shape is more like traditional QDs. On the other hand, a well-known shoulder is distinctive at high energies (wavelengths around 292 nm) due to the π-π* transitions of the sp2 π-conjugated core of the CQDs [70]. Since the energy shift between these two is remarkable, the longer-wavelength absorption can be attributed to the localized defect level [71] or non-bonding orbitals of surface sites [72]. The PLE spectrum also reveals strong excitation signals at 446 nm and 298 nm, which are in complete accordance with the UV-Vis result. To evaluate the emission properties, the PL spectrum was recorded at the excitation wavelength of 440 nm, showing a broad (FWHM= 98 nm) and strong signal located at 550 nm. First of all, the peak position shows

a very large Stokes shift of more than 100 nm related to the absorption peak which confirms the determinative role of localized midgap states in optical recombination. On the other hand, the position of the PL spectrum is not dependent on the excitation wavelength (as shown in the inset of Figure 6.1A), implying the presence of uniform radiative centers. It showed the best emission intensity recorded at an excitation wavelength of 440 nm, as expected from PLE's longer peak position. To verify the number of energy levels contributing to the recombination process, and the average emission lifetime, TRPL measurement was performed (Figure 6.1B). It demonstrates a decay profile well-matched with a single-exponential pathway and relatively long lifetime of 10.23 ns, assigned to the midgap radiative recombination centers [73]. This mono exponential behavior also shows a minimal role of trap-contributed recombination and fine uniformity of emissive centers [74]. The PLQY was measured via the comparative method (by choosing Rhodamine 6G with PL peak located at 560 nm, as the reference dye) for both as-synthesized and purified CQDs, showing a remarkable enhancement from 39% to 54%, respectively, with the approximately similar peak position, as reported elsewhere [75].

By evaluation of the effect of molecular weight on optical properties of similar CQDs structure, Guo et al. showed that PL characteristics are related to the size of CQDs which is normally observed in conventional QDs. Therefore, choosing the name of CQDs can be appropriate for present study[76]. Direct images of the purified CQDs under daylight and a 365 nm UV lamp have been provided Figure 6.1C emphasizing the bright yellow emission. Table 1 summarizes the PL emission features of the purified CQDs and compares them with other reports in the field confirming the luminescent merits of the prepared CQDs. For any practical application, the PL emission should be stable with long-time durability against harsh conditions.

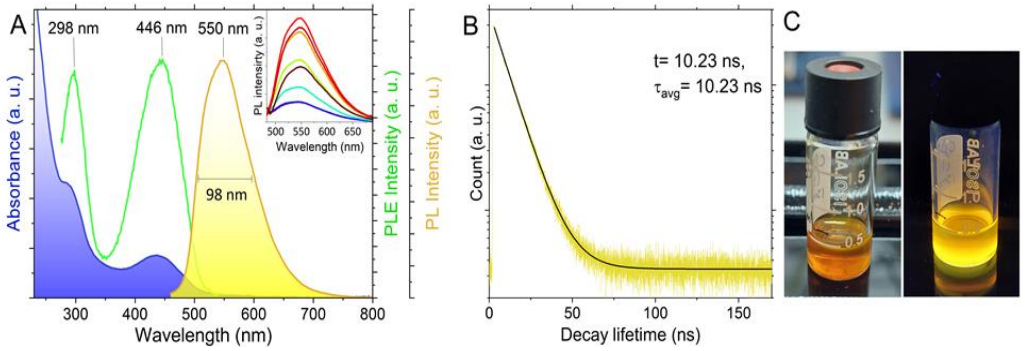

Figure 6.1 A) UV-Vis, PLE (λ ems=550 nm), and PL (λ exc=440 nm) spectra of purified CQDs. The inset shows the excitation-dependent PL spectrum recording from 340-to-480 nm. B) The logarithmic TRPL profile of the corresponding CQDs at the wavelength of 371 nm. The inset shows the fitting parameters. C) Digital images of the purified CQDs, under daylight and 365 nm UV irradiation.

While showing a broad PL signal with a large FWHM value is not generally attractive for optoelectronic purposes, due to the coverage of almost all the visible spectrum, it is becoming a unique property of CQDs to directly reach a high-performance WLED. In this case, an organic semiconductor is introduced as the host material to avoid π–π stacking of carbon dots in solid film form [77]–[79]. Due to its large bandgap and neat film-forming properties, a host-guest blend of CQDs doped PVK is used as an emission layer (EML) to fabricate CQDs-LED to further evaluate the electroluminescent properties. The device configuration is shown as an inset in Figure 6.2A, and it comprises, from up to the bottom, the layers of aluminum (Al) cathode, lithium fluoride (LiF) electron buffer layer, 1,3,5-tris(N-phenylbenzimidazol-2-yl)benzene (TPBi) electron transport layer, PVK:CQDs emitting layer, TFB hole transport layer, PEDOT:PSS hole injection layer, and indium-tin-oxide (ITO) anode. Figure 6.2B shows the normalized EL spectra of the CQD-LEDs, fabricated with different volume ratios of CQDs in PVK solution, at different driving voltages where the maximum luminescence occurs. The spectra of the CQD-LEDs prepared with different volume ratios will change accordingly, but in all cases, there are various peaks (shoulders) related to PVK and CQDs. Depending on the CQD:PVK ratio, the main emission peak of the EL spectra is located around 433-437 nm, and this blue emission originates from PVK. While the second one which is located at around 550 nm originated from the CQDs. Furthermore, by a change in the volume ratio of CQDs-to-PVK, the intensity ratio of these differentiated peaks also

changes due to the partial exciton transfer and electroluminescence from both CQD and PVK.

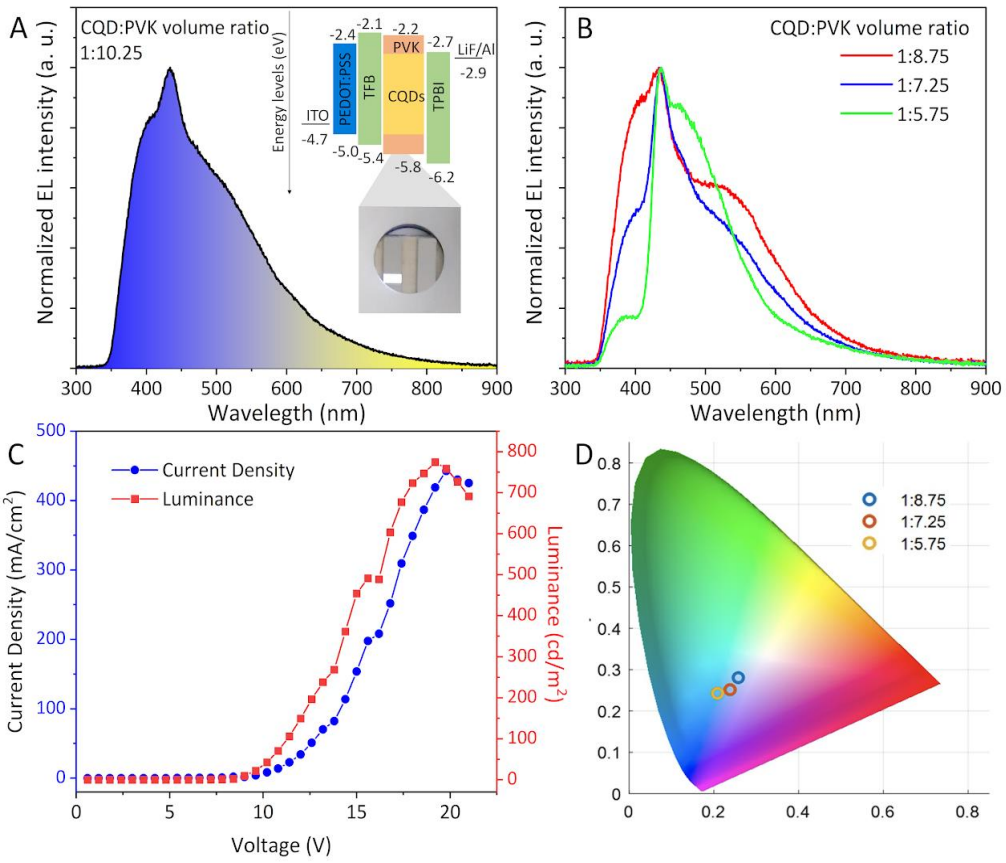

Figure 6.2 A) The CQD-LEDs normalized EL spectra (with a ratio of the volume of 1:10.25) and inset illustrations of the device's design photograph at a 14.4 V operating voltage. B) The normalized EL spectra of CQD-LED (with volume ratios of 1:8.75, 1:7.25, and 1:5.75) at a driving voltage of 14.4 V. C) The J–V–L characteristics curve of the CQD-LED (with a volume ratio of 1:10.25). D) The CIE coordinates of the CQD-LED (with volume ratios of 1:8.75, 1:7.25, and 1:5.75) at the driving voltage of 14.4 V.

The current density-voltage-luminance (J-V-L) characteristics of the CQD-LED (with a volume ratio of 1:10.25) that has the highest luminance are given in Figure 6.2C. The current density and the luminance increase under a driving voltage of 9.0-21.0 V, and the maximum luminance of 774.3 cd/m^2 is achieved at a driving voltage of 19.2 V, with the CIE coordinates of (0.23, 0.26). Ultimately, the CIE coordinates of CQD-LEDs with different volume ratios are calculated, which are presented in Figure 6.2D. When the volume ratios of CQD:PVK are 1:10.25, 1:8.75, 1:7.25, and 1:5.75, respectively, the

relevant CIE coordinates are situated at (0.23, 0.26), (0.26, 0.28), (0.24, 0.25), and (0.21, 0.24), which shows that by changing the volume ratio of the CQD in PVK solution color of the devices can be modified. To compare the presented electroluminescent results in this study with the reported literature, Table 6.1 has been included indicating good results for WLEDs fabricated by the CQDs.

Table 6.1 Comparison of the previous studies that have used CQD:PVK mixture as the light emitting layer (driving voltage is 14.4 V) with the present study.

Device structure	**Color**	**V_{on} (V)**	**L_{max} (cd/m^2)**	**EQE (%)**	**CIE (x,y)**	**Ref**
ITO/PVK:CQDs/TPBI or TmPyPB/LiF/Al	White	~8	339.5	-	0.41, 0.48	[80]
ITO/PEDOT:PSS/PVK:CQDs/ TPBi/Ca/Al	Multi	3.5	1882-4762	-	-	[81]
ITO/PEDOT:PSS/PVK:HCP-DB-CQDs/TPBi/Ca/Al	Blue	5-8	5240	4	0.15, 0.05	[82]
ITO/PEDOT:PSS/PVK:CQDs/ TPBI/Liq/Al	Blue	6.7	648	2.1	0.14, 0.10	[83]
ITO/PEDOT:PSS/PVK:CQDs/ TPBI/Liq/Al	White	3.6	626	1.18	0.33, 0.33	[84]
ITO/PEDOT:PSS/PVK:Y-CQDs/TPBI/LiF/Al	White	4.0	1718	0.004-0.18	0.48, 0.42	[85]

ITO/PEDOT:PSS/TFB/PVK:CQDs/TPBI/Liq/Al	Green		681	0.18	0.35, 0.53	[86]
ITO/PEDOT:PSS/TFB/PVK:CQDs/TPBI/Liq/Al	Yellow-Green	9.9	220	0.18	0.30, 0.65	[87]
ITO/PEDOT:PSS/PVK:CQDs/TPBI/Liq/Al	Blue	8.17	176	-	0.17, 0.10	[88]
ITO/PEDOT:PSS/TFB/PVK:CQDs/TPBI/LiF/Al	White	8.4*	774.3	0.35	0.23, 0.26	Present study
		9	223.6	0.28	0.26, 0.28	
		8.4	267.3	0.23	0.24, 0.25	
		6	391.8	0.76	0.21, 0.24	

* From top to bottom, the CQDs:PVK ratios in the present work are 1:10.25, 1:8.75, 1:7.25, and 1:5.75, respectively.

6.5 Conclusion

In this work, yellow emissive CQDs with PLQY of 60% were synthesized through a solvothermal method followed by column chromatography-assisted purification. The

purified samples showed an excitation-wavelength-independent PL peak position with a mono-exponential TRPL profile of 10.23 ns, showing the optical merits of the prepared samples. CQDs are suitable for solution-processed device applications, and PVK is introduced as a host to reduce the aggregation problem of CQDs in solid-state form. By adjusting the volume ratio between CQD and PVK, a shift in CIE x-y coordinates from 0.23-0.26 to 0.21-0.24 is realized. As the volume ratio of CQD:PVK solution changes from 1:5.75 to 1:8.75, CIE coordinate shifts from the blue region to the white region. White CQD-LEDs show L_{max} and EQEs values vary between 223.6-774.3 cd/m^2 and 0.23-0.76 percent, respectively. These results pave the way for the systematic engineering of the white light using CQDs.

Chapter 7

Cadmium Selenide QD LEDs

In terms of not containing heavy metal, InP and CQD are in the same group, but CdSe QDs contain cadmium heavy metal. Heavy are metallic elements that have a very high density compared to water (> 5 times). These materials are toxic materials and threaten life with factors such as physical and genetic disorders and cancer. Although it may seem dangerous, the important thing is the amount and duration of exposure [89]. Exposure is reduced by taking the necessary precautions during the fabrication of QLED devices and minimizing the contact with the outside by encapsulating them. Also, the inherent toxicity of core structures containing heavy metals, such as CdSe, can be decreased by using an appropriate shell structure, such as ZnS [90].

CdSe/ZnS QDs, whose recipe is given in the material synthesis section, are in type-I core/shell structure as mentioned in the previous sections. The ZnS shell in its structure has a positive effect on the material, as in other QDs, such as stability, solubility, and functionalization. As shown in Figure 2.2, the energy diagrams of electrons and holes overlap in the type-I QD structure, which has a positive effect on device efficiency.

The produced CdSe QDs are used as emitting layer in the QLED device structure. As mentioned in the previous sections, device structures are also divided into types according to whether the material used is organic or not. Type-IV device structure contains both organic and inorganic layers material. Type-IV structure can be categorized as conventional (Figure 7.1) or inverted (Figure 7.2) structure according to the side where electron and hole transport layers are located [91]. In the conventional structure, there are anode, hole injection layer, hole transport layer, emitting layer, electron transport layer and cathode, respectively. In the inverted structure, there are cathode, electron transport layer, emitting layer, hole transport layer, hole injection layer and anode, respectively. In

the device characterization, while applying potential difference, the positive terminal is connected by the anode and the negative terminal is connected by the cathode.

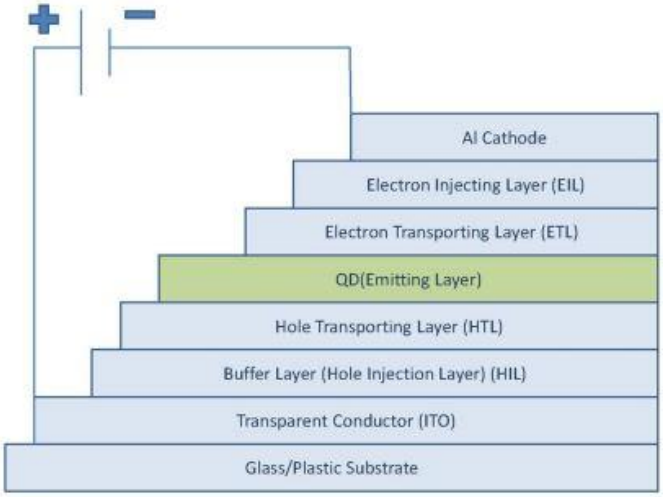

Figure 7.1 Conventional QLED device structure [91]

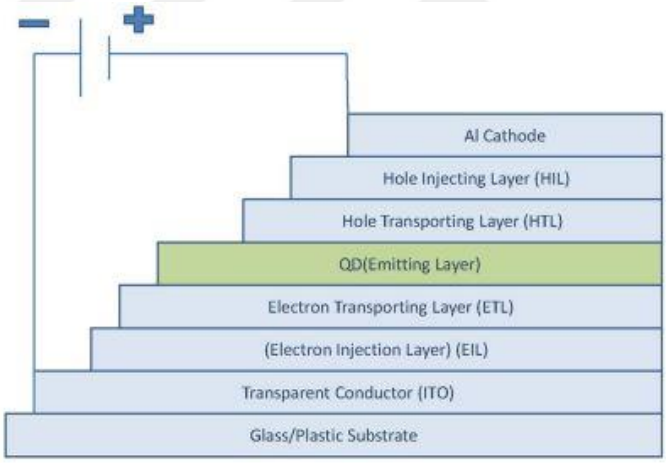

Figure 7.2 Inverted QLED device structure [91]

In this study, conventional QLED devices in Type-IV device structure were produced as proof of concept by using green CdSe/ZnS QDs. The devices were characterized by performing layer architecture optimization in the produced devices.

7.1 Fabrication

CdSe/ZnS QLED devices have undergone similar fabrication steps as InP and CQD QLED devices. It is first sonicated in boiled DI water, boiled DI water, and isopropyl to which Hellmanex-III is added, respectively, and then dried with nitrogen gas. Immediately after, the hole injection layer, PEDOT:PSS, is coated with the plasma cleaner from contamination. Then it is taken to the glovebox and covered in the form of PVK, QD and ZnO solution, respectively. Aluminum, which is the cathode, is coated at 100 nm by thermal evaporation. Fabrication details are as in Table 7.1. The device layer architecture is as shown in Figure 7.3.

Table 7.1 Device fabrication recipe

Layer	Concentration	Solvent	Spin Duration	Spin Speed	Annealing Temperature	Annealing Duration
PEDOT:PSS	12,64 mg/ml (before filtering)	Water	1.step: 3 s 2.step: 57 s	1.step: 3500 rpm 2.step: 5000 rpm	150°C	15 min
PVK	6 mg/ml	Chloroform	60 s	3000 rpm	150°C	30 min
QD	10 mg/ml	Hexane	30 s	1500 rpm	60°C	15 min
ZnO	20 mg/ml	Ethanol	60 s	2000 rpm	80°C	30 min
Cathode	Aluminum - 100 nm					

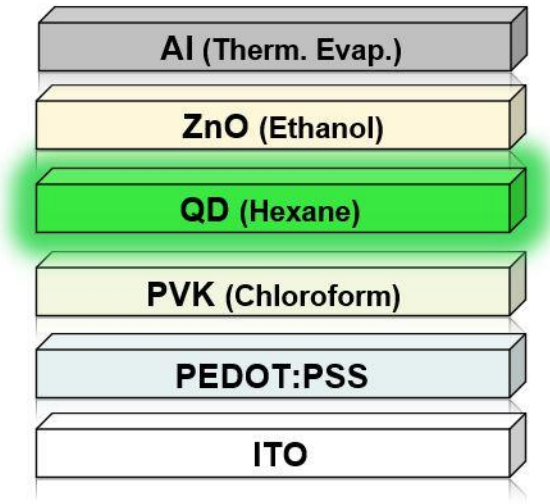

Figure 7.3 Fabricated Device structure

7.2 Characterization

Characterization was carried out using an integrating sphere, a Keithley 2400 source meter, and a Hamamatsu PMA-12 photonic multichannel analyzer. These equipment have been used to measure the device's brightness, EL, EQE, and current density values.

7.3 Results and Discussion

As a result of the work carried out, the maximum luminance of 111.450 cd/m^2 (Figure 7.4) and the maximum EQE of 15.08% were obtained in the devices produced. In addition to these, maximum current efficiency of 60.18 cd/A and maximum power efficiency of 28.65 lm/W were obtained. These are proof of concept device results with good luminosity and efficiency in terms of using CdSe/ZnS QDs from II-VI group examples in device structure.

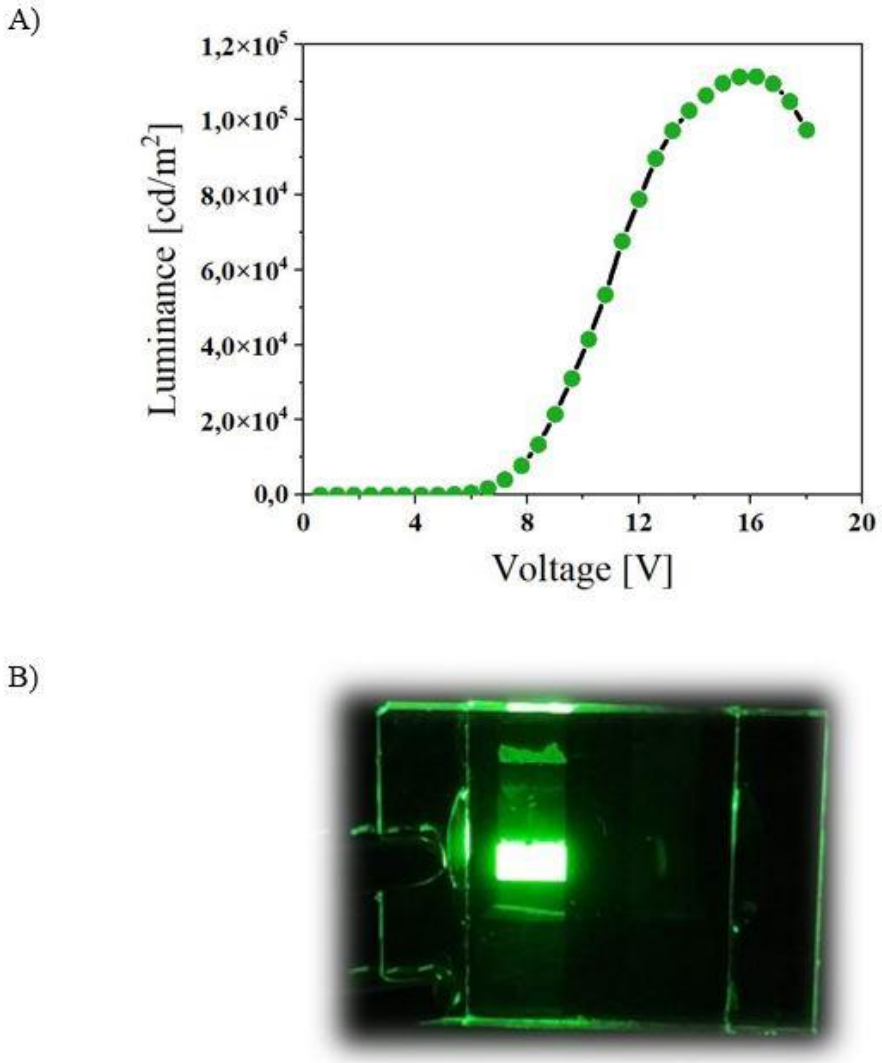

Figure 7.4 A) Luminance-Voltage graph of CdSe/ZnS QLED B) Device photo under applied voltage.

Chapter 8

Conclusion and Future Perspective

8.1 Conclusions

As mentioned in the first chapters, quantum dots and quantum dot LEDs have been the subject of many studies with their high luminous power, efficiency and rich diversity. The classification of quantum dots can be done on many grounds. They can be classified according to whether the material in their content is heavy metal or according to the group in the periodic table. In this thesis, 3 types of quantum dots are mentioned.

Firstly, devices with a maximum brightness of 1039 cd/m^2 and an EQE of 1.16% were produced by using InP/ZnSe/ZnS quantum dots as the emitting layer in the QLED structure, radiating in the deep red region of the CIE x-y coordinates (0.69-0.30).

Another study was carried out by mixing Carbon quantum dots into PVK and using them in the device structure. The CD:PVK ratio was added to the PVK as the host, with a ratio of 1:10.25, 1:8.75, 1:7.25, and 1:5.75, respectively, and used in the QLED structure as the emitting layer. It has been observed that blue-to-white shift occurs at varying mixing ratios. The CIE coordinates of this radiation are (0.23, 0.26), (0.26, 0.28), (0.24, 0.25), and (0.21, 0.24) with increasing CD amount. It has a maximum brightness of 774.3 cd/m^2 and fulfilling brightness with an EQE of 0.76% compared to devices of similar device architecture and glow color.

Finally, devices that glow green with a maximum brightness of 111,450 cd/m^2 were produced by using CdSe/ZnS quantum dots, which have been widely studied in the literature, as emitting layer in the Type-IV conventional device structure. It has also been observed that irradiation is efficient with an EQE of 15.08% in these devices.

8.2 Societal Impact and Contribution to Global Sustainability

QLED performance has been significantly improved since the first device was introduced. Thanks to its many advantageous features, QLEDs have recently attracted great attention for lighting and display applications. The increasing demand for these products, which is one of the most basic requirements of the digital age we live in, provides infrastructure directly to some of the UN Sustainable Development Goals [92] and indirectly to some.

The UN Sustainable Development Goals set 17 goals for the protection of the world and for people to live in a fairer and better way as they deserve. These goals are of a wide scale and variety [93]. Contributing to the realization of these goals with the work done is important in terms of sustainability. In this respect, the study, development and production of QLEDs are related to and serve these goals.

In order to produce QLEDs and integrate them into display technology products, both R&D studies and projects carried out in universities and technology centers and their transfer to industrial production are required. These innovations and productions on the basis of nanotechnology require cooperation and infrastructure. The work carried out in this cooperation directly contributes to the 9th 'Industry, Innovation and Infrastructure' goals of the UN Sustainable Development Goals, by enabling the industry to grow and develop, as well as innovative projects and productions.

With the developing industry and innovative studies, the features of production can only be possible with the presence of more employees. Having more employees in each unit creates an employment area. In addition, the work provided in an industrial environment, an environment where human rights are protected and good opportunities are offered, positively changes the working conditions of many people. In terms of these gains, it provides "Decent Work" and "Economic Growth" by providing added value to the economy with increasing employment and production. This contributes to the 8th UN goals.

QLED devices have a brighter and richer color gamut with less energy in terms of high efficiency. In addition, it enables the target of 'Affordable and Clean Energy', which is the 7th item, with very low-cost materials such as Carbon QDs used in production.

Since QLED studies and production can be carried out with potential partners from all over the world, as well as contributing to developing countries with factors such as industry, employment, and economic growth, it addresses the 17th 'Partnership for Goals' goal.

8.3 Future Prospects

In future studies, more efficient devices can be made and converted into products by structural optimization of devices, functional optimization of quantum dots, potential new materials or blending of existing materials [4]. More efficient products are vital in both user-friendly and mission-critical areas.

BIBLIOGRAPHY

[1] T. Maxwell, M. G. Nogueira Campos, S. Smith, M. Doomra, Z. Thwin, and S. Santra, "Quantum Dots," *Nanoparticles for Biomedical Applications: Fundamental Concepts, Biological Interactions and Clinical Applications*, pp. 243–265, Jan. 2020, doi: 10.1016/B978-0-12-816662-8.00015-1.

[2] W. M. Girma, M. Z. Fahmi, A. Permadi, M. A. Abate, and J. Y. Chang, "Synthetic strategies and biomedical applications of I–III–VI ternary quantum dots," *J Mater Chem B*, vol. 5, no. 31, pp. 6193–6216, Aug. 2017, doi: 10.1039/C7TB01156C.

[3] R. A. Freedman and W. J. Kaufmann, "Universe," 2008.

[4] N. Bastami, E. Soheyli, A. Arslan, R. Sahraei, A. F. Yazici, and E. Mutlugun, "Nanowire-Shaped MoS2@MoO3Nanocomposites as a Hole Injection Layer for Quantum Dot Light-Emitting Diodes," *ACS Appl Electron Mater*, vol. 4, no. 8, pp. 3849–3859, Aug. 2022, doi: 10.1021/ACSAELM.2C00485/ASSET/IMAGES/LARGE/EL2C00485_0007.JPEG.

[5] M. Savas, A. F. Yazıcı, A. A. Arslan, E. Mutlugün, and T. Erdem, "Toward sustainable optoelectronics: solution-processed quantum dot photodetector fabrication using a surgical blade," *https://doi.org/10.1117/1.OE.62.2.027102*, vol. 62, no. 2, p. 027102, Feb. 2023, doi: 10.1117/1.OE.62.2.027102.

[6] J. Kwak *et al.*, "Bright and efficient full-color colloidal quantum dot light-emitting diodes using an inverted device structure," *Nano Lett*, vol. 12, no. 5, pp. 2362–2366, May 2012, doi: 10.1021/NL3003254/SUPPL_FILE/NL3003254_SI_001.PDF.

[7] X. Dai, Y. Deng, X. Peng, and Y. Jin, "Quantum-Dot Light-Emitting Diodes for Large-Area Displays: Towards the Dawn of Commercialization," *Advanced Materials*, vol. 29, no. 14, p. 1607022, Apr. 2017, doi: 10.1002/ADMA.201607022.

[8] S. Y. Lim, W. Shen, and Z. Gao, “Carbon quantum dots and their applications,” *Chem Soc Rev*, vol. 44, no. 1, pp. 362–381, Dec. 2014, doi: 10.1039/C4CS00269E.

[9] Z. Cui *et al.*, “Advances, Challenges, and Perspectives for Heavy-Metal-Free Blue-Emitting Indium Phosphide Quantum Dot Light-Emitting Diodes,” *Adv Opt Mater*, vol. 11, no. 4, p. 2202036, Feb. 2023, doi: 10.1002/ADOM.202202036.

[10] S. Busatto and C. De Mello Donega, “Magic-Size Semiconductor Nanostructures: Where Does the Magic Come from?,” *ACS Materials Au*, 2021, doi: 10.1021/ACSMATERIALSAU.1C00075/ASSET/IMAGES/LARGE/MG1C00075_0010.JPEG.

[11] A. N. Yadav, A. K. Singh, and K. Singh, “Synthesis, Properties, and Applications of II–VI Semiconductor Core/Shell Quantum Dots,” pp. 1–28, 2020, doi: 10.1007/978-3-030-46596-4_1.

[12] K. B. Male, B. Lachance, S. Hrapovic, G. Sunahara, and J. H. T. Luong, “Assessment of cytotoxicity of quantum dots and gold nanoparticles using cell-based impedance spectroscopy,” *Anal Chem*, vol. 80, no. 14, pp. 5487–5493, Jul. 2008, doi: 10.1021/AC8004555/ASSET/IMAGES/LARGE/AC-2008-004555_0006.JPEG.

[13] J. Li and J. J. Zhu, “Quantum dots for fluorescent biosensing and bio-imaging applications,” *Analyst*, vol. 138, no. 9, pp. 2506–2515, Apr. 2013, doi: 10.1039/C3AN36705C.

[14] A. M. Stoneham, “Non-radiative transitions in semiconductors,” *Reports on Progress in Physics*, vol. 44, no. 12, p. 1251, Dec. 1981, doi: 10.1088/0034-4885/44/12/001.

[15] A. C. Bartnik, F. W. Wise, A. Kigel, and E. Lifshitz, “Electronic structure of PbSePbS core-shell quantum dots,” *Phys Rev B Condens Matter Mater Phys*, vol. 75, no. 24, p. 245424, Jun. 2007, doi: 10.1103/PHYSREVB.75.245424/FIGURES/5/MEDIUM.

[16] J. Yang *et al.*, "CdSeTe/CdS Type-I Core/Shell Quantum Dot Sensitized Solar Cells with Efficiency over 9%," *Journal of Physical Chemistry C*, vol. 119, no. 52, pp. 28800–28808, Dec. 2015, doi: 10.1021/ACS.JPCC.5B10546/ASSET/IMAGES/LARGE/JP-2015-10546Q_0007.JPEG.

[17] J. Sanmartín-Matalobos *et al.*, "Semiconductor Quantum Dots as Target Analytes: Properties, Surface Chemistry and Detection," *Nanomaterials 2022, Vol. 12, Page 2501*, vol. 12, no. 14, p. 2501, Jul. 2022, doi: 10.3390/NANO12142501.

[18] P. Reiss, M. Protière, and L. Li, "Core/Shell Semiconductor Nanocrystals," *Small*, vol. 5, no. 2, pp. 154–168, Jan. 2009, doi: 10.1002/SMLL.200800841.

[19] J. Cho, Y. K. Jung, J. K. Lee, and H. S. Jung, "Highly efficient Blue-Emitting CdSe-derived Core/Shell Gradient Alloy Quantum Dots with Improved Photoluminescent Quantum Yield and Enhanced Photostability," *Langmuir*, vol. 33, no. 15, pp. 3711–3719, Apr. 2017, doi: 10.1021/ACS.LANGMUIR.6B04333/ASSET/IMAGES/LA-2016-04333W_M003.GIF.

[20] Y. Zhou, H. Zhao, D. Ma, and F. Rosei, "Harnessing the properties of colloidal quantum dots in luminescent solar concentrators," *Chem Soc Rev*, vol. 47, no. 15, pp. 5866–5890, Jul. 2018, doi: 10.1039/C7CS00701A.

[21] M. A. Jhonsi and M. A. Jhonsi, "Carbon Quantum Dots for Bioimaging," *State of the Art in Nano-bioimaging*, Jun. 2018, doi: 10.5772/INTECHOPEN.72723.

[22] C.-Y. Han, H. Yang, C.-Y. Han, and H. Yang, "Development of Colloidal Quantum Dots for Electrically Driven Light-Emitting Devices," *Journal of the Korean Ceramic Society*, vol. 54, no. 6, pp. 449–469, Nov. 2017, doi: 10.4191/KCERS.2017.54.6.03.

[23] T. Tsujimura, "OLED Display Fundamentals and Applications," *OLED Display Fundamentals and Applications*, Apr. 2017, doi: 10.1002/9781119187493.

[24] R. A. J. Janssen and J. W. Stouwdam, “Red, green, and blue quantum dot LEDs with solution processable ZnO nanocrystal electron injection layers,” *J Mater Chem*, vol. 18, no. 16, pp. 1889–1894, Apr. 2008, doi: 10.1039/b800028j.

[25] M. K. Choi, J. Yang, T. Hyeon, and D. H. Kim, “Flexible quantum dot light-emitting diodes for next-generation displays,” *npj Flexible Electronics 2018 2:1*, vol. 2, no. 1, pp. 1–14, Apr. 2018, doi: 10.1038/s41528-018-0023-3.

[26] P. C. Chiu and S. H. Yang, “Improvement in hole transporting ability and device performance of quantum dot light emitting diodes,” *Nanoscale Adv*, vol. 2, no. 1, pp. 401–407, Jan. 2020, doi: 10.1039/C9NA00618D.

[27] V. Wood, M. J. Panzer, J. E. Halpert, J. M. Caruge, M. G. Bawendi, and V. Bulović, “Selection of metal oxide charge transport layers for colloidal quantum dot LEDs,” *ACS Nano*, vol. 3, no. 11, pp. 3581–3586, Nov. 2009, doi: 10.1021/NN901074R/ASSET/IMAGES/LARGE/NN-2009-01074R_0003.JPEG.

[28] J. Li, Y. Shao, X. Chen, H. Wang, Y. Li, and Q. Zhang, “All-inorganic quantum-dot light-emitting-diodes with vertical nickel oxide nanosheets as hole transport layer,” *Progress in Natural Science: Materials International*, vol. 26, no. 5, pp. 503–509, Oct. 2016, doi: 10.1016/J.PNSC.2016.09.003.

[29] Y. Shang and Z. Ning, “Colloidal quantum-dots surface and device structure engineering for high-performance light-emitting diodes,” *Natl Sci Rev*, vol. 4, no. 2, pp. 170–183, Mar. 2017, doi: 10.1093/NSR/NWW097.

[30] N. Tu, “Quantum Dot Light-Emitting Diode: Structure, Mechanism, and Preparation,” *Quantum Dots - Fundamental and Applications*, Jun. 2020, doi: 10.5772/INTECHOPEN.91162.

[31] V. L. Colvin, M. C. Schlamp, and A. P. Alivisatos, “Light-emitting diodes made from cadmium selenide nanocrystals and a semiconducting polymer,” *Nature 1994 370:6488*, vol. 370, no. 6488, pp. 354–357, 1994, doi: 10.1038/370354a0.

[32] H. Mattoussi, L. H. Radzilowski, B. O. Dabbousi, E. L. Thomas, M. G. Bawendi, and M. F. Rubner, “Electroluminescence from heterostructures of poly(phenylene vinylene) and inorganic CdSe nanocrystals,” *J Appl Phys*, vol. 83, no. 12, pp. 7965–7974, Jun. 1998, doi: 10.1063/1.367978.

[33] B. O. Dabbousi, M. G. Bawendi, O. Onitsuka, and M. F. Rubner, “Electroluminescence from CdSe quantum-dot/polymer composites,” *Appl Phys Lett*, p. 1316, 1995, doi: 10.1063/1.113227.

[34] V. Wood and V. Bulović, “Colloidal quantum dot light-emitting devices,” *http://dx.doi.org/10.3402/nano.v1i0.5202*, vol. 1, no. 1, p. 5202, Jan. 2010, doi: 10.3402/NANO.V1I0.5202.

[35] J. Zhao *et al.*, “Efficient CdSe/CdS quantum dot light-emitting diodes using a thermally polymerized hole transport layer,” *Nano Lett*, vol. 6, no. 3, pp. 463–467, Mar. 2006, doi: 10.1021/NL052417E/SUPPL_FILE/NL052417ESI20060113_084524.PDF.

[36] S. Coe, W. K. Woo, M. Bawendi, and V. Bulović, “Electroluminescence from single monolayers of nanocrystals in molecular organic devices,” *Nature 2002 420:6917*, vol. 420, no. 6917, pp. 800–803, Dec. 2002, doi: 10.1038/nature01217.

[37] A. H. Mueller *et al.*, “Multicolor light-emitting diodes based on semiconductor nanocrystals encapsulated in GaN charge injection layers,” *Nano Lett*, vol. 5, no. 6, pp. 1039–1044, Jun. 2005, doi: 10.1021/NL050384X/SUPPL_FILE/NL050384XSI20050301_113926.PDF.

[38] J. M. Caruge, J. E. Halpert, V. Wood, V. Buloví, and M. G. Bawendi, “Colloidal quantum-dot light-emitting diodes with metal-oxide charge transport layers,” *Nature Photonics 2008 2:4*, vol. 2, no. 4, pp. 247–250, Mar. 2008, doi: 10.1038/nphoton.2008.34.

[39] N. Tu and N. Tu, “Quantum Dot Light-Emitting Diode: Structure, Mechanism, and Preparation,” *Quantum Dots - Fundamental and Applications*, Mar. 2020, doi: 10.5772/INTECHOPEN.91162.

[40] J. M. Caruge, J. E. Halpert, V. Bulović, and M. G. Bawendi, “NiO as an inorganic hole-transporting layer in quantum-dot light-emitting devices,” *Nano Lett*, vol. 6, no. 12, pp. 2991–2994, Dec. 2006, doi: 10.1021/NL0623208/ASSET/IMAGES/MEDIUM/NL0623208N00001.GIF.

[41] Y. J. Han, K. T. Kang, B. K. Ju, and K. H. Cho, “Effect of Time-Dependent Characteristics of ZnO Nanoparticles Electron Transport Layer Improved by Intense-Pulsed Light Post-Treatment on Hole-Electron Injection Balance of Quantum-Dot Light-Emitting Diodes,” *Materials 2020, Vol. 13, Page 5041*, vol. 13, no. 21, p. 5041, Nov. 2020, doi: 10.3390/MA13215041.

[42] L. Qian, Y. Zheng, J. Xue, and P. H. Holloway, “Stable and efficient quantum-dot light-emitting diodes based on solution-processed multilayer structures,” *Nat Photonics*, vol. 5, no. 9, pp. 543–548, Aug. 2011, doi: 10.1038/nphoton.2011.171.

[43] Q. Yuan, T. Wang, P. Yu, H. Zhang, H. Zhang, and W. Ji, “A review on the electroluminescence properties of quantum-dot light-emitting diodes,” *Org Electron*, vol. 90, p. 106086, Mar. 2021, doi: 10.1016/J.ORGEL.2021.106086.

[44] Y. Sun, Q. Su, H. Zhang, F. Wang, S. Zhang, and S. Chen, “Investigation on Thermally Induced Efficiency Roll-Off: Toward Efficient and Ultrabright Quantum-Dot Light-Emitting Diodes,” *ACS Nano*, vol. 13, no. 10, pp. 11433–11442, Oct. 2019, doi: 10.1021/ACSNANO.9B04879/ASSET/IMAGES/LARGE/NN9B04879_0005.JPEG.

[45] L. Qian *et al.*, “Electroluminescence from light-emitting polymer/ZnO nanoparticle heterojunctions at sub-bandgap voltages,” *Nano Today*, vol. 5, no. 5, pp. 384–389, Jan. 2010, doi: 10.1016/J.NANTOD.2010.08.010.

[46] Y. Altintas, S. Genc, M. Y. Talpur, and E. Mutlugun, “CdSe/ZnS quantum dot films for high performance flexible lighting and display applications,” *Nanotechnology*, vol. 27, no. 29, p. 295604, Jun. 2016, doi: 10.1088/0957-4484/27/29/295604.

[47] M. Guo, K. Zhang, X. Zhu, and H. Li, “Optical losses of CdS films on FTO, ITO, and AZO electrodes in CdTe–HgCdTe tandem solar cells,” *Journal of Materials Science: Materials in Electronics*, vol. 26, no. 10, pp. 7607–7613, Oct. 2015, doi: 10.1007/S10854-015-3397-1/TABLES/1.

[48] “(7) The State of ITO Alternatives: Why Your Next Innovative Printed Electronics Product Will Use CNT Hybrid Films | LinkedIn.” https://www.linkedin.com/pulse/state-ito-alternatives-why-your-next-innovative-use-cnt-ken-klapproth/ (accessed May 06, 2023).

[49] M. Chrzanowski, M. Banski, P. Sitarek, J. Misiewicz, and A. Podhorodecki, “Quantum-dot light-emitting diode with ultrathin Au electrode embedded in solution-processed phosphomolybdic acid,” *RSC Adv*, vol. 9, no. 19, pp. 10754–10759, Apr. 2019, doi: 10.1039/C9RA01680E.

[50] K. Ding *et al.*, “24.1% External Quantum Efficiency of Flexible Quantum Dot Light-Emitting Diodes by Light Extraction of Silver Nanowire Transparent Electrodes,” *Adv Opt Mater*, vol. 6, no. 19, p. 1800347, Oct. 2018, doi: 10.1002/ADOM.201800347.

[51] “ITO Glass Substrates | 20 x 15 mm (Legacy, Generation I) | Ossila.” https://www.ossila.com/products/oled-ito-substrates (accessed May 07, 2023).

[52] Y. Park, V. Choong, Y. Gao, B. R. Hsieh, and C. W. Tang, “Work function of indium tin oxide transparent conductor measured by photoelectron spectroscopy,” *Appl Phys Lett*, vol. 68, no. 19, pp. 2699–2701, May 1996, doi: 10.1063/1.116313.

[53] I. D. Parker and A. Phys Lett, “Carrier tunneling and device characteristics in polymer light-emitting diodes,” *J Appl Phys*, vol. 75, no. 3, pp. 1656–1666, Feb. 1994, doi: 10.1063/1.356350.

[54] Y. Park, V. Choong, Y. Gao, B. R. Hsieh, and C. W. Tang, “Work function of indium tin oxide transparent conductor measured by photoelectron spectroscopy,” *Appl Phys Lett*, vol. 68, no. 19, pp. 2699–2701, May 1996, doi: 10.1063/1.116313.

[55] M. S. Farhan, E. Zalnezhad, A. R. Bushroa, and A. A. D. Sarhan, “Electrical and optical properties of indium-tin oxide (ITO) films by ion-assisted deposition (IAD) at room temperature,” *International Journal of Precision Engineering and Manufacturing*, vol. 14, no. 8, pp. 1465–1469, Aug. 2013, doi: 10.1007/S12541-013-0197-5/METRICS.

[56] “ITO Glass Substrates | 20 x 15 mm (Legacy, Generation I) | Ossila.” https://www.ossila.com/products/oled-ito-substrates (accessed May 07, 2023).

[57] W. Cao *et al.*, “Highly stable QLEDs with improved hole injection via quantum dot structure tailoring,” *Nature Communications 2018 9:1*, vol. 9, no. 1, pp. 1–6, Jul. 2018, doi: 10.1038/s41467-018-04986-z.

[58] J. G. Calvert, “Glossary of atmospheric chemistry terms,” *Pure and Applied Chemistry*, vol. 62, no. 11, pp. 2167–2219, Jan. 1990, doi: 10.1351/PAC199062112167/MACHINEREADABLECITATION/RIS.

[59] W. Zhang *et al.*, “Effect of chalcogen substitution on aqueous dispersions of poly(3,4-ethylenedioxythiophene)s:poly(4-styrenesulfonate) and their flexible conducting films,” *Journal of Materials Science: Materials in Electronics*, vol. 29, no. 21, pp. 18566–18572, Nov. 2018, doi: 10.1007/S10854-018-9973-4.

[60] “Self-healing metal oxides could protect against corrosion | MIT News | Massachusetts Institute of Technology.” https://news.mit.edu/2018/self-healing-metal-oxides-could-protect-against-corrosion-0404 (accessed May 07, 2023).

[61] K. P. Acharya, A. Titov, J. Hyvonen, C. Wang, J. Tokarz, and P. H. Holloway, “High efficiency quantum dot light emitting diodes from positive aging,” *Nanoscale*, vol. 9, no. 38, pp. 14451–14457, Oct. 2017, doi: 10.1039/C7NR05472F.

[62] Z. Chen, Q. Su, Z. Qin, and S. Chen, “Effect and mechanism of encapsulation on aging characteristics of quantum-dot light-emitting diodes,” *Nano Res*, vol. 14, no. 1, pp. 320–327, Jan. 2021, doi: 10.1007/S12274-020-3091-3/METRICS.

[63] I. Tanaka and S. Tokito, “Precise measurement of external quantum efficiency of organic light-emitting devices,” *Japanese Journal of Applied Physics, Part 1: Regular Papers and Short Notes and Review Papers*, vol. 43, no. 11 A, pp. 7733–7736, Nov. 2004, doi: 10.1143/JJAP.43.7733/XML.

[64] “Luminance, explained by RP Photonics Encyclopedia; photometry, units, brightness, radiance.” https://www.rp-photonics.com/luminance.html (accessed May 07, 2023).

[65] S. Scholz, D. Kondakov, B. Lüssem, and K. Leo, “Degradation mechanisms and reactions in organic light-emitting devices,” *Chem Rev*, vol. 115, no. 16, pp. 8449–8503, Aug. 2015, doi: 10.1021/CR400704V/ASSET/IMAGES/CR400704V.SOCIAL.JPEG_V03.

[66] “(2) (PDF) 2018 DOE Solid-State Lighting R&D Opportunities.” https://www.researchgate.net/publication/330545079_2018_DOE_Solid-State_Lighting_RD_Opportunities (accessed May 07, 2023).

[67] Y. H. Won *et al.*, “Highly efficient and stable InP/ZnSe/ZnS quantum dot light-emitting diodes,” *Nature 2019 575:7784*, vol. 575, no. 7784, pp. 634–638, Nov. 2019, doi: 10.1038/s41586-019-1771-5.

[68] W. K. Bae *et al.*, “Controlled alloying of the core-shell interface in CdSe/CdS quantum dots for suppression of auger recombination,” *ACS Nano*, vol. 7, no. 4, pp. 3411–3419, Apr. 2013, doi: 10.1021/NN4002825/SUPPL_FILE/NN4002825_SI_001.PDF.

[69] J. R. Lakowicz, “Principles of fluorescence spectroscopy,” p. 698, 1999.

[70] T. Li, W. Shi, Q. Mao, and X. Chen, “Regulating the photoluminescence of carbon dots via a green fluorine-doping-derived surface-state-controlling strategy,” *J Mater Chem C Mater*, vol. 9, no. 48, pp. 17357–17364, Dec. 2021, doi: 10.1039/D1TC04660H.

[71] G. Zheng *et al.*, "Localized Excitonic Electroluminescence from Carbon Nanodots," *Journal of Physical Chemistry Letters*, vol. 13, no. 6, pp. 1587–1595, Feb. 2022, doi: 10.1021/ACS.JPCLETT.1C04028/SUPPL_FILE/JZ1C04028_SI_001.PDF.

[72] J. Joseph and A. A. Anappara, "Cool white, persistent room-temperature phosphorescence in carbon dots embedded in a silica gel matrix," *Physical Chemistry Chemical Physics*, vol. 19, no. 23, pp. 15137–15144, Jun. 2017, doi: 10.1039/C7CP02731A.

[73] Y. Chen *et al.*, "Concentration-induced multi-colored emissions in carbon dots: origination from triple fluorescent centers," *Nanoscale*, vol. 10, no. 14, pp. 6734–6743, Apr. 2018, doi: 10.1039/C8NR00204E.

[74] F. Yuan *et al.*, "Bright high-colour-purity deep-blue carbon dot light-emitting diodes via efficient edge amination," *Nature Photonics 2019 14:3*, vol. 14, no. 3, pp. 171–176, Dec. 2019, doi: 10.1038/s41566-019-0557-5.

[75] K. Sato, R. Katakami, Y. Iso, and T. Isobe, "Surface-Modified Carbon Dots with Improved Photoluminescence Quantum Yield for Color Conversion in White-Light-Emitting Diodes," *ACS Appl Nano Mater*, vol. 5, no. 6, pp. 7664–7669, Jun. 2022, doi: 10.1021/ACSANM.2C01868/SUPPL_FILE/AN2C01868_SI_001.PDF.

[76] J. Guo *et al.*, "Yellow-Emissive Carbon Dots with High Solid-State Photoluminescence," *Adv Funct Mater*, vol. 32, no. 20, p. 2110393, May 2022, doi: 10.1002/ADFM.202110393.

[77] F. Yuan *et al.*, "Bright Multicolor Bandgap Fluorescent Carbon Quantum Dots for Electroluminescent Light-Emitting Diodes," *Advanced Materials*, vol. 29, no. 3, p. 1604436, Jan. 2017, doi: 10.1002/ADMA.201604436.

[78] H. Jia *et al.*, "Electroluminescent Warm White Light-Emitting Diodes Based on Passivation Enabled Bright Red Bandgap Emission Carbon Quantum Dots,"

Advanced Science, vol. 6, no. 13, p. 1900397, Jul. 2019, doi: 10.1002/ADVS.201900397.

[79] W. Kwon *et al.*, "Electroluminescence from graphene quantum dots prepared by amidative cutting of tattered graphite," *Nano Lett*, vol. 14, no. 3, pp. 1306–1311, Mar. 2014, doi: 10.1021/NL404281H/SUPPL_FILE/NL404281H_SI_001.PDF.

[80] J. Xu, Y. Miao, J. Zheng, H. Wang, Y. Yang, and X. Liu, "Carbon dot-based white and yellow electroluminescent light emitting diodes with a record-breaking brightness," *Nanoscale*, vol. 10, no. 23, pp. 11211–11221, Jun. 2018, doi: 10.1039/C8NR01834K.

[81] F. Yuan *et al.*, "Engineering triangular carbon quantum dots with unprecedented narrow bandwidth emission for multicolored LEDs," *Nature Communications 2018 9:1*, vol. 9, no. 1, pp. 1–11, Jun. 2018, doi: 10.1038/s41467-018-04635-5.

[82] F. Yuan *et al.*, "Bright high-colour-purity deep-blue carbon dot light-emitting diodes via efficient edge amination," *Nature Photonics 2019 14:3*, vol. 14, no. 3, pp. 171–176, Dec. 2019, doi: 10.1038/s41566-019-0557-5.

[83] X. Wang *et al.*, "Ultra-Bright and Stable Pure Blue Light-Emitting Diode from O, N Co-Doped Carbon Dots," *Laser Photon Rev*, vol. 15, no. 3, p. 2000412, Mar. 2021, doi: 10.1002/LPOR.202000412.

[84] X. Wang *et al.*, "Carbon-Dot-Based White-Light-Emitting Diodes with Adjustable Correlated Color Temperature Guided by Machine Learning," *Angewandte Chemie International Edition*, vol. 60, no. 22, pp. 12585–12590, May 2021, doi: 10.1002/ANIE.202103086.

[85] Z. Wang, N. Jiang, M. Liu, R. Zhang, F. Huang, and D. Chen, "Bright Electroluminescent White-Light-Emitting Diodes Based on Carbon Dots with Tunable Correlated Color Temperature Enabled by Aggregation," *Small*, vol. 17, no. 52, p. 2104551, Dec. 2021, doi: 10.1002/SMLL.202104551.

[86] Z. Zheng *et al.*, "Structural Engineering toward High Monochromaticity of Carbon Dots-Based Light-Emitting Diodes," *Journal of Physical Chemistry Letters*, vol. 12, no. 50, pp. 12107–12113, Dec. 2021, doi: 10.1021/ACS.JPCLETT.1C03786/SUPPL_FILE/JZ1C03786_SI_001.PDF.

[87] Y. Ding *et al.*, "Preparation and luminescent modulation of yellow carbon dots for electroluminescent device," *J Lumin*, vol. 249, p. 119036, Sep. 2022, doi: 10.1016/J.JLUMIN.2022.119036.

[88] T. Zhang *et al.*, "Carbon dots promote the carrier recombination in Poly (9-vinyl carbazole) to enhance its electroluminescence," *Appl Surf Sci*, vol. 585, p. 152649, May 2022, doi: 10.1016/J.APSUSC.2022.152649.

[89] G. J. Supran *et al.*, "QLEDs for displays and solid-state lighting," *MRS Bull*, vol. 38, no. 9, pp. 703–711, Sep. 2013, doi: 10.1557/MRS.2013.181/FIGURES/7.

[90] R. Bogue, "Quantum dots: A bright future for photonic nanosensors," *Sensor Review*, vol. 30, no. 4, pp. 279–284, 2010, doi: 10.1108/02602281011072143/FULL/XML.

[91] P. Kathirgamanathan, L. M. Bushby, S. Surendrakumar, M. Kumaraverl, and S. Ravichandran, "Electroluminescent Organic and Quantum Dot LEDs: The State of the Art," *Journal of Display Technology, Vol. 11, Issue 5, pp. 480-493*, vol. 11, no. 5, pp. 480–493, May 2015, doi: 10.1109/JDT.2015.2418279.

[92] "THE 17 GOALS | Sustainable Development." https://sdgs.un.org/goals (accessed Jul. 12, 2023).

[93] "Sustainable Development Goals." https://www.who.int/europe/about-us/our-work/sustainable-development-goals (accessed Jul. 12, 2023).

CURRICULUM VITAE

Education:

2015 – 2019 B.Sc., Electrical and Electronics Engineering, Abdullah Gul University, Kayseri, TURKEY

2020 – Present Sc., Electrical and Computer Engineering, Abdullah Gul University, Kayseri, TURKEY

SELECTED PUBLICATIONS AND PRESENTATIONS

J1) Nasim Bastami, Ehsan Soheyli, Ayşenur Arslan, Reza Sahraei, Ahmet Faruk Yazici, and Evren Mutlugun, Nanowire-Shaped MoS2@MoO3 Nanocomposites as a Hole Injection Layer for Quantum Dot Light-Emitting Diodes published in ACS Applied Electronic Materials (Aug. 2022)

J2) Muzeyyen Savas, Ahmet Faruk Yazici, Aysenur Arslan, Evren Mutlugün, Talha Erdem, Toward sustainable optoelectronics: solution-processed quantum dot photodetector fabrication using a surgical blade published in Optical Engineering (Feb. 2023)

C1) M. Savas, A. F. Yazici, A. Arslan, E. Mutlugün, and T. Erdem, Simple, sustainable fabrication of fully solution-processed, transparent, metalsemiconductor-metal photodetectors using a surgical blade as an alternative to conventional tools (May 2022)